arXiv:1409.5043v4 [hep-ex] 5 Mar 2015

REVIEW OF PHYSICS RESULTS FROM THE TEVATRON: HIGGS BOSON PHYSICS

Thomas R. Junk

Fermi National Accelerator Laboratory
Batavia, Illinois 60510, United States of America
trj@fnal.gov

Aurelio Juste

Institució Catalana de Recerca i Estudis Avançats (ICREA) and
Institut de Física d'Altes Energies (IFAE)
Edifici Cn, Facultat de Ciencies
Universitat Autònoma de Barcelona
E-08193 Bellaterra (Barcelona), Spain
juste@ifae.es

12 February, 2015

We review the techniques and results of the searches for the Higgs boson performed by the two Tevatron collaborations, CDF and DØ. The Higgs boson predicted by the Standard Model was sought in the mass range 90 GeV$< m_H <$ 200 GeV in all main production modes at the Tevatron: gluon-gluon fusion, WH and ZH associated production, vector boson fusion, and $t\bar{t}H$ production, and in five main decay modes: $H \to b\bar{b}$, $H \to \tau^+\tau^-$, $H \to WW^{(*)}$, $H \to ZZ^{(*)}$, and $H \to \gamma\gamma$. An excess of events was seen in the $H \to b\bar{b}$ searches consistent with a Standard Model Higgs boson with a mass in the range 115 GeV$< m_H <$135 GeV. Assuming a Higgs boson mass of $m_H = 125$ GeV, studies of Higgs boson properties were performed, including measurements of the product of the cross section times the branching ratio in various production and decay modes, constraints on Higgs boson couplings to fermions and vector bosons, and tests of spin and parity. We also summarize the results of searches for supersymmetric Higgs bosons, and Higgs bosons in other extensions of the Standard Model.

Keywords: Tevatron, CDF, D0, Higgs boson

PACS numbers: 13.85.Rm, 14.80.Bn, 14.80.Da, 14.80.Ec, 14.80.Fd

Contents

1. Introduction 3
2. Higgs Boson Theory and Phenomenology 4
   2.1. Standard Model Higgs boson production 4
   2.2. Standard Model Higgs boson decay 5
   2.3. Precision electroweak constraints and direct searches 6
   2.4. Higgs bosons in extensions of the Standard Model 7
3. Analysis Tools 7
   3.1. Particle identification 8

3.2. Jet identification and energy measurement . . . 8
3.3. b-Tagging . . . 9
3.4. Missing energy . . . 10
3.5. Top quark identification and reconstruction . . . 10
3.6. Multivariate analyses . . . 11
3.7. Statistical methods . . . 12
4. Searches for the Standard Model Higgs Boson . . . 15
4.1. Search strategies . . . 15
4.2. Signal and background modeling . . . 16
4.3. Searches for $H \to b\bar{b}$ . . . 17
4.3.1. $WH \to \ell\nu b\bar{b}$ . . . 18
4.3.2. $ZH \to \ell^+\ell^- b\bar{b}$ . . . 19
4.3.3. $WH, ZH \to \not{E}_T b\bar{b}$ . . . 20
4.3.4. $VH(\to b\bar{b})$ search results and validation . . . 20
4.3.5. $VH, q\bar{q}H \to jjb\bar{b}$ . . . 22
4.3.6. $t\bar{t}H \to t\bar{t}b\bar{b}$ . . . 22
4.4. Searches for $H \to \tau^+\tau^-$ . . . 22
4.5. Searches for $H \to WW^{(*)}$ . . . 23
4.5.1. Opposite-sign dileptons . . . 23
4.5.2. Same-sign dileptons and trileptons . . . 26
4.5.3. Lepton-plus-jets . . . 26
4.5.4. $H \to WW^{(*)}$ search results and validation . . . 26
4.6. Searches for $H \to ZZ^{(*)}$ . . . 27
4.7. Searches for $H \to \gamma\gamma$ . . . 27
4.8. Standard Model Higgs boson search results . . . 28
4.8.1. Limits . . . 29
4.8.2. Significance . . . 30
4.8.3. Cross section fits . . . 31
4.8.4. Coupling constraints . . . 31
4.8.5. Tests of spin and parity . . . 32
5. Searches for Higgs Bosons Beyond the Standard Model . . . 34
5.1. Heavy neutral Higgs bosons decaying to vector bosons . . . 34
5.2. Heavy neutral Higgs bosons decaying to fermions . . . 36
5.2.1. $\phi \to b\bar{b}$ . . . 37
5.2.2. $\phi \to \tau^+\tau^-$ . . . 38
5.3. Charged Higgs bosons . . . 39
5.4. Light CP-odd Higgs bosons . . . 41
5.5. Doubly-charged Higgs bosons . . . 42
5.6. Higgs boson decays to hidden-sector particles . . . 43
6. Summary and Conclusions . . . 44

1. Introduction

The recent observation of the Higgs boson by the ATLAS and CMS Collaborations at the Large Hadron Collider[1,2] closes a long chapter in experimental particle physics and begins a new one in which the properties of the Higgs boson are used to test for new physical phenomena. In 1964 the existence of a massive scalar boson became a key testable prediction of the Higgs mechanism,[3–6] which is the simplest description of how the observed masses of the W and Z gauge bosons, as well as those of the fermions, are consistent with the $\mathrm{SU}(2)_L \times \mathrm{U}(1)_Y$ gauge symmetry. This symmetry, when broken by the Higgs mechanism to the $\mathrm{U}(1)_{\mathrm{EM}}$ symmetry of quantum electrodynamics, provides the basis of the Standard Model (SM),[7–9] a very successful framework that predicts, or at least accommodates, all particle physics measurements made to date. The mysteries of dark matter, dark energy, and a quantum description of gravity remain beyond the scope of the SM, though the Higgs bosons produced in the laboratory can be a window to testing alternate hypotheses motivated by these unexplained phenomena. For many years, the non-observation of exotic particles, Higgs bosons among them, have constrained many possible models of new physics.

The search for Higgs bosons was a central component of the Run II physics program at the Tevatron. Early estimates of the sensitivity[10,11] indicated that tests of the presence or absence of the SM Higgs boson were achievable, even though these estimates were uncertain due to the level of precision of the available signal cross section predictions as well as the rudimentary estimates and handling of backgrounds rates, signal efficiencies, and systematic uncertainties. Models of exotic Higgs boson production provided motivation to search for Higgs bosons even with smaller data sets. Many of the upgrades to the Tevatron and the two detectors, CDF and DØ, described elsewhere in this review, were motivated by the Higgs boson physics program, though these upgrades also had positive impacts on the broad physics objectives of the two collaborations.

With the full Tevatron Run II data set, CDF and DØ combined their search results together and in July 2012 obtained the first evidence for a particle produced in association with vector bosons and which decays to $b\bar{b}$, consistent with the expectation for the SM Higgs boson.[12] Measurements of the cross sections times decay branching ratios in different production and decay modes, as well as tests of couplings and spin and parity, were performed.[13–16] No significant deviations from the predictions for the SM Higgs boson with a mass near 125 GeV were seen. Because the Tevatron searches were most sensitive to processes in which the Higgs boson decays to fermion pairs, they are naturally complementary with the LHC searches, which are most sensitive to decays of the Higgs boson to pairs of bosons ($\gamma\gamma$, $ZZ^{(*)}$, and $WW^{(*)}$). This article describes the components of the Tevatron searches for the Higgs boson and their interpretation, starting with the models under test, and proceeding with the experimental equipment, analysis tools, and results.

2. Higgs Boson Theory and Phenomenology

The simplest implementation of the Higgs mechanism is that used by the SM. A doublet of self-interacting complex scalar fields is introduced that, by virtue of the opposite sign of the quadratic and quartic terms in the Higgs potential, acquires a vacuum expectation value at the minimum of the potential, which has a three-dimensional degeneracy. This degeneracy would result in three massless Goldstone bosons, which are not observed. Instead, the three degrees of freedom appear as the longitudinal polarization components of the W^+, W^-, and Z bosons, endowing these particles with their masses. The fourth degree of freedom has finite-mass excitations corresponding to a neutral scalar boson H with a mass m_H that is not predicted by the theory. Together with the gauge interactions of the SM, the Higgs mechanism completes the model by allowing for both fermion and gauge boson masses while preserving renormalizability.[17]

2.1. *Standard Model Higgs boson production*

At tree level in the SM, the Higgs boson couples to a species of fermion with a strength proportional to that fermion's mass, and to a species of boson with a strength proportional to the square of that boson's mass. This feature, along with the kinematic availability of each final state, determines the decay branching ratios of the SM Higgs boson as a function of its mass. The dominant decay modes are to the heaviest particles kinematically available, with a preference for decays to massive bosons. The couplings of the Higgs boson to SM particles tend to be smaller than electroweak and strong couplings, leading to the challenge of searching for rare Higgs boson processes among much more copious backgrounds.

At one loop and higher, the Higgs boson couples to the massless gauge bosons g and γ, even though the tree-level couplings vanish. The Hgg coupling is dominated by a top-quark loop, although the b-quark loop also contributes a non-negligible amount. The presence of additional gluons radiated by the gluons coupling to the Higgs boson increases both the $gg \to H$ production cross section at hadron colliders, and the decay branching ratio for $H \to gg$. Gluon radiation also modifies the branching ratios of the Higgs boson to quarks. Because of the small couplings of the Higgs boson to the u and d quarks, the primary constituents of the proton, the $gg \to H$ production mechanism is the dominant process at both the Tevatron and the LHC. The sub-dominant processes are production in association with a vector boson ($q\bar{q} \to WH, ZH$, referred to as VH), as well as vector boson fusion (VBF) ($q\bar{q} \to q'\bar{q}'H$), and Yukawa radiation from a top quark pair ($t\bar{t}H$) or a b-quark pair ($b\bar{b}H$), the latter of which can be dominant in extensions of the SM with enhanced couplings to down-type quarks. More rare modes include production in association with a single top quark and the production of a pair of Higgs bosons.

The SM predictions of the production rates in $p\bar{p}$ collisions are shown as functions of m_H in Fig. 1(a). The $gg \to H$ production rate is computed at next-to-next-to-leading order (NNLO) with next-to-next-to-leading-logarithmic (NNLL) soft-gluon

summation accuracy in QCD (referred to as NNLO+NNLL),[18–27] including the effects of mixed QCD-electroweak corrections and the running b-quark mass. Higher-order corrections are very important in this process due to the strong coupling of gluons to additional particles: the next-to-leading order (NLO) k-factor is approximately 2.0, and at NNLO, there is an additional factor of ~ 1.5. A partial calculation at next-to-next-to-next-to-leading order (NNNLO) in QCD[28] provides some confidence that the corrections from further terms in the series become smaller, and are adequately covered by the factorization and renormalization scale uncertainties customarily assigned. The parton distribution functions (PDFs) used in the cross section calculations used for the Tevatron results are the MSTW2008 set[29] and the recommended uncertainties.[30,31] The differential spectrum of $gg \to H$ production is complex and has experimental consequences. The production rates for $gg \to H + 1$ jet and $gg \to H + \geq 2$ jets have been calculated at NLO in QCD,[32,33] and the p_T spectrum at NLO+NNLL.[34–36]

The theoretical uncertainty on the total production rate for $gg \to H$ is approximately $\pm 10\%$,[26,27] although the uncertainty on the production rate for $gg \to H$+jets is significantly larger – it is $\pm 23\%$ for the ≥ 2 jets category. The CDF and DØ Collaborations follow the procedure of Ref. 37 in order to account for the correlations (positive and negative) between the predictions of the rates in the exclusive observable jet categories used to analyze the data. The impact of the factorization and renormalization scale uncertainties on the PDF uncertainties are considered correlated with the factorization and renomalization scale uncertainties and are added linearly with those. The remaining components of the PDF uncertainties are considered uncorrelated.

For the associated production cross sections, $p\bar{p} \to WH + X$ and $p\bar{p} \to ZH + X$, the CDF and DØ Collaborations use the calculations of Ref. 38, which are performed at NNLO precision in QCD and NLO precision in electroweak corrections. A similar calculation is available in Ref. 39. The theoretical uncertainties in these predictions are approximately $\pm 8\%$ at m_H=125 GeV, mostly due to the PDF uncertainties.

The VBF cross section is computed at NNLO in QCD,[40] and the electroweak corrections are computed with the HAWK program.[41] The $t\bar{t}H$ production cross sections are computed at NLO in QCD,[42–44] although this last cross section calculation was computed using the CTEQ6M PDF set.[45]

2.2. *Standard Model Higgs boson decay*

The decay branching ratios to pairs of particles are shown in Fig. 1(b).[47] Refinements to these calculations are provided in Refs. 48 and 49. These are obtained by using the HDECAY program[50] to compute the partial widths for all decay modes except the four-fermion final states resulting from the $H \to WW^{(*)}$ and $H \to ZZ^{(*)}$ decay modes, which interfere quantum mechanically. These latter contributions are computed using PROPHECY4F.[51] The partial widths are then summed and the fractions of the total widths are the resulting branching ra-

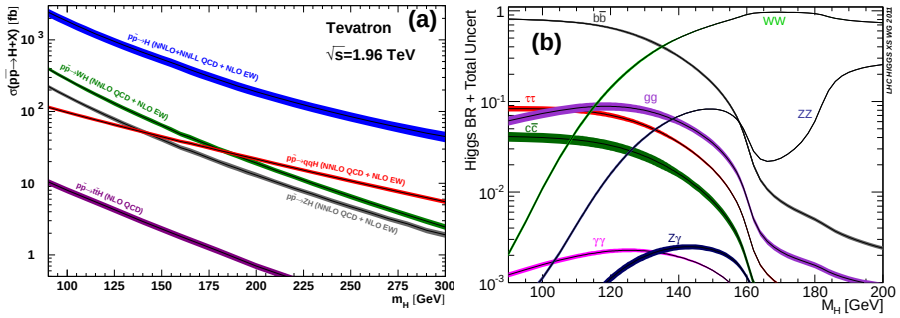

Fig. 1. (a) Production cross sections for the gluon-fusion process (labeled $p\bar{p} \to H$), the WH, ZH, VBF (labeled $p\bar{p} \to qqH$), and $t\bar{t}H$ processes. From Ref. 46. (b) Decay branching fractions for the SM Higgs boson as functions of its mass. From Ref. 47.

tios. Uncertainties in the branching ratios are assessed from uncertainties in the masses of the final state particles, specifically the b and c quark masses, and the factorization and renormalization scale uncertainties used to estimate the effects of missing higher order terms in the calculation. At $m_H = 125$ GeV, the SM predictions for the branching ratios are approximately:[47] $\mathcal{B}(H \to b\bar{b}) \approx 57.8\%$, $\mathcal{B}(H \to WW^{(*)}) \approx 21.6\%$, $\mathcal{B}(H \to \tau^+\tau^-) \approx 6.37\%$, $\mathcal{B}(H \to \gamma\gamma) \approx 0.23\%$, $\mathcal{B}(H \to gg) \approx 8.56\%$, $\mathcal{B}(H \to ZZ^{(*)}) \approx 0.23\%$, and $\mathcal{B}(H \to Z\gamma) \approx 0.16\%$.

2.3. *Precision electroweak constraints and direct searches*

Searches by the four LEP collaborations excluded $m_H < 114.4$ GeV at the 95% confidence level (C.L.), assuming SM properties of the Higgs boson, taking advantage of the associated production mode, $e^+e^- \to ZH$.[52,53] LEP also placed strong limits on the production of additional Higgs bosons predicted by the minimal supersymmetric standard model (MSSM),[54,55] which can provide visible signatures even when the coupling strengths of the ZH and Zh processes are suppressed.[56] LEP sought a great variety of Higgs boson decay final states explicitly, such as $H \to \gamma\gamma$,[57] $H \to$ hadrons[58] and $H \to$ invisible,[59] in addition to the SM and MSSM searches. The limit on the mass of the SM Higgs boson from LEP provides a lower bound in the region of interest for the Tevatron searches, although those searches were extended down to $m_H = 90$ GeV, largely to validate the modeling of the lower-mass Higgs boson searches, and to make a point of comparison with the corresponding measurements of non-resonant diboson production, WZ and ZZ, described in Sec. 4.3.4.

Precision electroweak measurements also provide constraints on m_H assuming SM relations.[60] Combined with the precision measurements of the top quark mass m_t[61] and the W boson mass M_W,[62] an upper bound of $m_H < 152$ GeV is obtained at the 95% C.L. Adding in the constraint from direct LEP searches raises the upper bound to $m_H < 171$ GeV at the 95% C.L.

2.4. *Higgs bosons in extensions of the Standard Model*

The observation of a SM-like Higgs boson at the LHC has established the existence of a state of the electroweak symmetry breaking sector, but it has not proven that the minimal SM Higgs mechanism provides a full description of it. In fact, many extensions of the SM postulate the existence of an extended scalar Higgs sector. For instance, introducing a second Higgs doublet, such as in Two Higgs Doublet Models (2HDM),[63,64] leads to five physical Higgs bosons: a light and a heavy CP-even Higgs boson (h and H), a CP-odd Higgs boson (A), and a pair of charged bosons ($H^{\pm}$). The MSSM is, at leading order, an example of a Type-II 2HDM, where up- and down-type quarks couple to separate Higgs doublets. CP violation in the MSSM Higgs sector[65,66] would relax the production selection rules and enlarge the possible space of parameters to search. The next-to-minimal MSSM (NMSSM)[67] further extends the MSSM to include an additional CP-even and CP-odd neutral Higgs bosons. In the NMSSM, the lightest CP-odd Higgs boson, a, can be very light, even below the $b\bar{b}$ threshold. Alternatively, Higgs triplet models extend the SM by adding a complex $\mathrm{SU}(2)_L$ triplet scalar field, predicting a pair of doubly-charged Higgs bosons ($H^{\pm\pm}$), in addition to the five Higgs bosons present in 2HDMs. Finally, some extensions of the SM predict the existence of massive metastable particles that can only decay to SM particles through diagrams containing a new high-mass force carrier or a loop of very massive particles. These scenarios, referred to as "hidden-valley" (HV) models,[68] can involve a HV scalar particle that can mix with the SM Higgs boson, so that the latter could decay with substantial branching ratio to HV particles.[69–71]

Additional particle content may be present to augment the SM's three generations of fermions and its set of gauge bosons. A model that consists of the SM with one additional generation of fermions is referred to as SM4.[72] The presence of two very heavy quarks would lead to an enhancement in the ggH coupling by a factor of approximately three, since each heavy quark Q would contribute as much as the top quark in the SM. The contributions to the ggH amplitude are nearly independent of the masses of the new heavy quarks as the suppression factors from the propagators cancel the enhancement from the QQH couplings.[73–75] The $gg \to H$ production cross section therefore rises by a factor of approximately nine relative to the SM prediction in the range of m_H the Tevatron is sensitive to, and the partial decay width of the Higgs boson to gluons also increases by a factor of nine. Even with a higher decay rate to a pair of gluons, the $H \to WW^{(*)}$ decay mode continues to dominate for $m_H > 135$ GeV.

3. Analysis Tools

The searches for the SM Higgs boson and Higgs bosons in exotic models are especially challenging due to the small signal production cross sections and the large background rates. The analyses reported here make extensive use of nearly every capability of the CDF and DØ detectors. As data were collected, the experience

gained in refining the tools was used to improve the sensitivity of the Higgs boson searches, so that over time the sensitivity increased significantly faster than expected from simple luminosity scaling.

3.1. *Particle identification*

Searches for $WH \to \ell\nu b\bar{b}$, $ZH \to \ell^+\ell^- b\bar{b}$, and $H \to WW^{(*)} \to \ell^+\nu\ell^-\bar{\nu}$ rely heavily on identifying leptons with high efficiency and low rates of backgrounds from misidentified jets. Typically, analyses are designed to select electrons and muons, as the detectors are optimized to separate these from hadronic backgrounds. Tracks in the CDF COT and the DØ fiber tracker are associated with EM showers in the calorimeters to identify electrons and with track segments in the surrounding muon chambers to identify muons. Activity in the hadronic calorimeters inconsistent with electrons or muon signatures is used to veto hadrons that otherwise might pass the lepton identification selections, and the spatial distribution of the energy in the electromagnetic calorimeters is also used as a discriminating variable, helping to reduce the background from $\pi^0 \to \gamma\gamma$ decays misidentified as electrons. Lepton candidates are categorized in terms of their quality – how many selection requirements they pass, and whether they are detected in the central portion of the detectors or the forward portions, or travel through uninstrumented materials. Isolated tracks are also counted as lepton candidates in some analyses; these channels are analyzed separately from the others so as not to dilute the purity of higher-quality lepton selections.

The lepton identification efficiencies and energy resolutions are calibrated using $Z \to e^+e^-$ and $Z \to \mu^+\mu^-$ samples in the data. Lepton triggers are based on identifying one lepton at a time, and so tag-and-probe methods are used to calibrate the trigger efficiencies: in $Z \to \ell^+\ell^-$ events in which one lepton satisfies the trigger requirements, the other is used to probe the trigger efficiency with minimal bias. Similar methods are used to calibrate the efficiencies of lepton identification requirements. Lepton energy scales are calibrated with leptonically-decaying Z, J/ψ, and Υ events.

3.2. *Jet identification and energy measurement*

Energy deposits in the electromagnetic and hadronic calorimeters are grouped into jets using a cone-based algorithm with a radius $\Delta R = 0.4$ (CDF) and 0.5 (DØ), where $\Delta R = \sqrt{(\Delta\eta)^2 + (\Delta\phi)^2}$ [a]. In many analyses, the charged particle momenta are measured for tracks within these jets and are combined with the calorimetric measurements in order to improve the energy resolution, a key ingredient to

[a]Both CDF and DØ use right-handed coordinate systems, with the z axis directed along the proton beam. The azimuthal angle ϕ around the beam axis is defined with respect to a horizontal ray running outwards from the center of the Tevatron, and radii are measured with respect to the beam axis. The polar angle θ is defined with respect to the proton beam direction, and the pseudorapidity η is defined to be $\eta = -\ln[\tan(\theta/2)]$.

the searches for $H \to b\bar{b}$. The jet energy scale is likewise important for the same searches. Not all of the energy of the hadrons in jets is measured by the calorimeters – some of it is absorbed in nuclear interactions, some of it leaks out the back of the calorimeters, and some of it falls outside of the jet cones. Data samples, such as dijets, photons recoiling against jets or $Z \to e^+e^-, \mu^+\mu^-$ recoiling against jets, are used to calibrate the response of the calorimeters and the jet algorithms to hadronic jets with known transverse momenta.[76,77] Typical resolutions for jet energies are of order 8%, with higher-E_T jets being better measured than lower-E_T jets. Jets originating from gluons at the hard-scatter vertex tend to be wider than jets originating from quarks, resulting in a different energy scale due to the jet identification and energy clustering algorithms.[78,79] Even though quark and gluon jets may be well simulated by parton-shower Monte Carlos (MC) such as PYTHIA, the application of a calorimetric energy correction factor derived on a data sample with a given fraction of quark jets to a sample with a different fraction is not correct; instead, two separate correction factors must be derived and applied separately to quark and gluon jets in the MC samples.

Jets containing B hadrons suffer from additional jet energy biases compared with light-flavored jets, due to the high masses of B hadrons which disperse the decay particles outside of the jet cones and also because semileptonic decays of B and D hadrons produce neutrinos whose momenta are not measured. Algorithms are devised to improve the jet energy scale and resolution specifically for b jets.[80]

3.3. *b-Tagging*

Searches for $WH \to Wb\bar{b}$ and $ZH \to Zb\bar{b}$ have large backgrounds from vector bosons producted in association with jets. The vast majority of these jets are light-flavored, and so separation of b jets from light-flavored jets provides a significant improvement in the signal-to-background ratio in these searches. Multivariate Algorithms (MVAs) are designed to key on the large mass (≈ 5 GeV) and long lifetimes (≈ 1.4 ps) of B hadrons. Charged tracks from B (and subsequent D) hadron decay tend to have significantly larger impact parameters with respect to the beam axis than tracks created promptly at the primary vertex, whose impact parameters are dominated by resolution effects and multiple scattering. Displaced vertices are identified topologically and their properties, such as the invariant masses of the contributing tracks, the decay length, and the presence of leptons are all used to separate b jets from light-flavored jets.[81–86] Typical performances achieved for b tagging are 50% efficiency for b jets from top quark decay with a 0.5% mistag rate of light-flavored jets in the same momentum range, for a typical tight operating point corresponding to a requirement on the MVA score. A benefit of using a continuous variable to rank jets as being more or less b-like is that multiple operating points of the tagger can be used within the analyses. A typical loose requirement yields a b-tagging efficiency of 80% with a mistag rate of 10%, although some of these jets are also tagged by the tighter requirements. Analyses are constructed out of the

exclusive subsets of tagged events. The b-tagging efficiencies and mistag rates are calibrated with data control samples such as $t\bar{t}$ decays, $W/Z + 1$ jet events (where the flavor composition is measured with other taggers), and multijet events.

3.4. *Missing energy*

Because the PDFs are broad, events can be boosted along the beam axis by an unknown amount. Therefore, unlike an e^+e^- collider, which typically has a known total three-momentum and energy of the interactions, only the sum of the transverse momenta is possible to constrain at a hadron collider. The $WH \to \ell\nu b\bar{b}$ channel and the $H \to WW^{(*)} \to \ell^+\nu\ell^-\bar{\nu}$ and the $WH \to WWW$ channels seek leptonically-decaying W bosons, and the accompanying high-momentum neutrinos are not reconstructed. The $ZH \to \nu\bar{\nu}b\bar{b}$ channel has two high-momentum neutrinos in each signal event. The presence of a lepton and missing transverse momentum, or merely missing transverse momentum by itself, are powerful discriminant variables for reducing backgrounds and selecting Higgs boson events. Since the recoiling system is often hadronic, the calorimetry is used to sum the visible energy in an event, and the angle from the primary vertex is used to compute the transverse projections of the calorimeter energies. The negative vector sum of these transverse energies is denoted $\vec{\not\!\!E}_T$, and its magnitude is $\not\!\!E_T$.

Because $\not\!\!E_T$ is an inference of unmeasured momenta from a sum of measurements that are subject to physical, detector, and reconstruction effects, its value is often rather different from the sum of the neutrino momenta it approximates. Jet energies are corrected for the jet energy scale as described in Sec. 3.2, although individual jet mismeasurement constitutes the main cause for $\not\!\!E_T$ mismeasurement. Frequently the difference between $\vec{\not\!\!E}_T$ and $\vec{\not\!\!p}_T$, where $\vec{\not\!\!p}_T$ is the missing momentum using the tracks measured by the tracking detectors, is used to help identify events with mismeasured $\not\!\!E_T$.

3.5. *Top quark identification and reconstruction*

The $t\bar{t}$ production cross section at the Tevatron is approximately 7 pb, significantly larger than the Higgs boson production cross section. Its decays, to $W^+bW^-\bar{b}$, can mimic the signal in all of the main search channels: $WH \to \ell\nu b\bar{b}$, $H \to WW^{(*)}$, $ZH \to \ell^+\ell^- b\bar{b}$, $WH + ZH \to \not\!\!E_T b\bar{b}$, and others, usually as a result of one or more of the decay products of one or both top quarks falling outside of the detector acceptance or being misreconstructed. The highest-purity $t\bar{t}$ samples involve more jets than are normally required of the Higgs boson searches, and thus e.g. rejecting events with four or more jets is effective at reducing the $t\bar{t}$ background in the $WH \to \ell\nu b\bar{b}$ searches. In the $H \to WW^{(*)} \to \ell^+\nu\ell^-\bar{\nu}$ search, the signal is not expected to contain b quarks, and so the b-tag requirement is inverted on reconstructed jets within the acceptance of the silicon detectors in order to reduce the $t\bar{t}$ background. Full reconstruction of top quarks is rarely needed in order to reject

events in which they may be present, particularly in cases in which particles are missing or mismeasured.

Single top quark production has a final state that is the same as that of the $WH \to \ell\nu b\bar{b}$ search, and it has a cross section of approximately 3 pb. Fortunately, the kinematics of single top quark production are quite striking. Variables such as m_{jj}, $m_{\ell\nu b}$ and $q \times \eta$, where q is the charge of the lepton and η is the pseudo-rapidity of the non-b-tagged jet[87] are quite powerful in separating single top quark production from Higgs boson production.

3.6. *Multivariate analyses*

The small predicted signal cross sections and the large non-resonant backgrounds to Higgs boson production require that all possible methods be used in order to distinguish signal-like events from background-like ones. The usual distinguishing feature – the invariant mass of reconstructed candidates, which ought to produce a localized excess in its distribution at the mass of the Higgs boson – is not a powerful enough variable to perform the searches only with it. In $H \to b\bar{b}$ searches, the dijet mass distribution is wide enough and the expected signal small enough that a noticeable excess would not be seen on top of the background. In the $H \to WW^{(*)} \to \ell^+\nu\ell^-\bar{\nu}$ searches, the invariant mass of the Higgs boson cannot be reconstructed with good resolution due to the missing neutrino momenta. Other variables, such as the transverse momentum of the dijet system, the missing transverse energy, or the angle between the two leptons in the $H \to WW^{(*)} \to \ell^+\nu\ell^-\bar{\nu}$ searches, help provide separation between the signal and the background

The relatively large systematic uncertainties in the background predictions would wash out a small potential signal if events were merely counted after applying selection cuts – it is impossible to discover or exclude a signal that is smaller than the uncertainty on the background. Furthermore, if an analysis were to simply select events and count them, different event selection requirements would need to be chosen in order to optimize the analysis for setting limits, making a discovery, and measuring the signal rate. Multivariate analysis techniques provide solutions to these challenges by scoring events according to how signal-like (or background-like) their measured properties are. Higgs boson searches at the Tevatron typically make use of neural networks,[88–90] boosted decision trees,[91] and matrix-element techniques.[92,93] Some analyses use several MVA discriminant functions sequentially in order to separate the signal from more than one distinct source of background contamination. Typically, signal and background MC samples are used to train MVA classifier functions, with event samples that are statistically independent from those used to predict the signal and background rates in the subsequent statistical analyses. In some analyses and for some discriminants, data events in background-enriched control samples (in which the signal contribution is expected to be negligible) are used in the background training samples.

The MVA discriminants are functions of reconstructed quantities for each event

and their distributions are used in the statistical analyses, as described in Sec. 3.7. Events falling in low signal-to-background portions of the MVA discriminant outputs serve as sideband constraints for the backgrounds, while events in the high signal-to-background regions provide the most powerful tests of the presence or absence of a Higgs boson, and measure its production rate. In the most sensitive Higgs boson searches, the signal predictions in the highest-score bins are much larger than the corresponding post-fit background uncertainties. Multiple MVA functions are used in order to separate background contributions from each other in order to reduce the total uncertainty on the background contributions by providing measurements of each component.

In order to optimize the sensitivity of the searches, separate MVA functions are trained at each hypothesized value of m_H, typically on a grid between 90 GeV and 200 GeV, in steps of 5 GeV. The input variables to the MVA selections are also optimized for each m_H value in some analyses. These differences give rise to some statistical fluctuations in the observed cross sections and limits as functions of m_H even though the sensitivity is expected to be a smooth function if all searches are optimized at each m_H.

3.7. *Statistical methods*

The statistical methods used to extract results from the Higgs boson searches at the Tevatron are described in Refs. 46 and 13. Both Bayesian and Modified Frequentist methods are used, and their results are compared to check that the conclusions reached do not depend significantly on the choice of statistical method. The methods are chosen to make maximum use of the separation power of the MVA techniques, while at the same time incorporating the effects of systematic uncertainties in the rates, shapes, and independent bin-by-bin uncertainties that arise from limited MC sample (or data control sample) statistics. The inclusion of uncertainties on the shapes of the distributions of complex MVA discriminant variables allays concerns that unmodeled shape distortions can give spurious results if only the rates of contributing signal and background contributions are allowed to vary. Shape distortions due to systematic uncertainties are estimated by holding the discriminant function fixed and varying the uncertain parameters in the modeling and producing alternate distributions for the variable in question. Examples are provided below.

Both the Bayesian and the Modified Frequentist techniques rely on a binned likelihood function of the data, the model parameters, and the nuisance parameters. In most analyses the model parameters are m_H and μ, a signal strength modifier which scales the SM predictions in all combined channels together. Each independent source of systematic uncertainty is assigned a nuisance parameter, and correlated systematic uncertainties are decomposed by their sources in order to assign independent parameters. The predictions of the yields in each bin for the expected signal and the backgrounds are itemized by process and they depend on the model parameters and the nuisance parameters. Some nuisance parameters, such

as the integrated luminosity, scale the predicted yields in each bin of all processes affected by them. In the case of the luminosity, this consists of all processes using theoretical predictions and MC models. Other parameters, such as the jet energy scale in the detector simulation and the QCD factorization and renormalization scale parameters in the event generators affect both the total rates of processes (due to the fraction of events passing the event selection requirements) and also the shapes of the predicted distributions of kinematic variables. Correlations are included by parameterizing all bins and all channels' predictions that are sensitive to a particular systematic effect by the same nuisance parameter. Each process in each bin is also subject to a random, independent uncertainty due to MC (or data from a control sample) statistics and given a separate nuisance parameter. In the searches presented here, sufficient MC samples have been simulated in order to render negligible the effects of limited MC statistics.

In the Bayesian method, the nuisance parameters are integrated over ("marginalized"):

$$L' = \int L(\text{data}|\vec{\theta},\vec{\nu})\pi(\vec{\nu})d\vec{\nu} \tag{1}$$

where $L(\text{data}|\vec{\theta},\vec{\nu})$ is the likelihood function of the data, $\vec{\theta}$ are the model parameters m_H and μ, and $\vec{\nu}$ are the nuisance parameters. Typically nuisance parameters are given Gaussian priors $\pi(\vec{\nu})$, truncated so that no prediction of any signal or background is negative, although more sophisticated priors are also possible. Studies have shown that in practical applications, the RMS widths of the prior distributions is the most important feature controlling the impact of a particular systematic uncertainty on the results.

The 95% credibility level (C.L.) upper limit on the rate μ of a process (μ_{limit}) is given by

$$0.95 = \frac{\int_0^{\mu_{\text{limit}}} L'(\text{data}|\mu)\pi(\mu)d\mu}{\int_0^{\infty} L'(\text{data}|\mu)\pi(\mu)d\mu} \tag{2}$$

where the prior probability distribution for μ is taken to be uniform [b]. Markov Chain MC techniques[94,95] are used to compute the integrals of Eqs. 1 and 2 efficiently. The sensitivity of the search is quantified by the expected limit, which is computed as the median limit in a sample of simulated datasets with only background processes contributing, sampling over the systematic uncertainties. Expected sensitivity calculations also include 68% and 95% probability intervals for the limits, computed with the same simulated pseudo-datasets. To measure cross sections, the maximum of the posterior probability density of μ, $L'(\text{data}|\mu)\pi(\mu)$, is found, and the uncer-

[b]There is a formal divergence in limits computed with truncated Gaussian priors and uniform priors on μ, although they hardly appear in practice as the integration ranges are typically chosen to be very large instead of infinite, and the sampling of the signal rates near zero is not infinitely fine.

tainty is quoted using the shortest interval containing 68% of the integral of the posterior density.

In the Modified Frequentist method, two p-values are computed using a log-likelihood ratio (LLR) as the test statistic:

$$\mathrm{LLR} = \frac{L(\mathrm{data}|\mu, \hat{\hat{\vec{\nu}}})}{L(\mathrm{data}|\mu = 0, \hat{\vec{\nu}})}. \tag{3}$$

Two maximum-likelihood fits are performed to the data, allowing the nuisance parameters $\vec{\nu}$ to float. One fit assumes that a signal is present with strength μ, and the best-fit nuisance parameters in this case are denoted $\hat{\hat{\vec{\nu}}}$, and the other fit is performed assuming a signal is absent ($\mu = 0$), and the corresponding best-fit nuisance parameters are denoted $\hat{\vec{\nu}}$. The two p-values are

$$\mathrm{CL_{s+b}} = p(\mathrm{LLR} \geq \mathrm{LLR_{obs}}|\mu) \tag{4}$$

and

$$\mathrm{CL_b} = p(\mathrm{LLR} \geq \mathrm{LLR_{obs}}|\mu = 0). \tag{5}$$

The impact of systematic uncertainties on the p-values is included by sampling the values of the nuisance parameters within their prior distributions in the process of generating pseudo-datasets in the calculation of the p-values. The p-value

$$1 - \mathrm{CL_b} = p(\mathrm{LLR} \leq \mathrm{LLR_{obs}}|\mu = 0) \tag{6}$$

is used to discover a new process. If it is small, then the ability of the null hypothesis to explain the data is small. Small p-values are reported in units of Gaussian significance z using the integral of one side of a Gaussian distribution:

$$p = (1 - \mathrm{erf}(z/\sqrt{2}))/2. \tag{7}$$

A significance z of 3 is the customary threshold for claiming evidence, and a significance of 5 is the threshold for claiming observation or discovery. These p-values are computed separately for each value of m_H and are called "local" p-values. The "Look-Elsewhere Effect" (LEE),[96,97] also called the multiple-tests effect, is taken into account by studying the distribution of the smallest $1 - \mathrm{CL_b}$ over a sample of simulated background-only datasets and the "global" p-value is the probability of obtaining a specific value of the smallest local p-value or smaller. The sensitivity of the search at a specific mass m_H is quantified by the median expected local p-value assuming a signal is truly present at that mass.

Limits on μ are obtained using the $\mathrm{CL_s}$ technique in addition to the Bayesian limits described above. The ratio $\mathrm{CL_s}$=$\mathrm{CL_{s+b}}/\mathrm{CL_b}$ is computed as a function of the signal strength modifier μ, and the upper limit on μ is defined to be that which yields $\mathrm{CL_s} = 0.05$. The median expected upper limit on μ and the 68% and 95% intervals of the distribution of the upper limit on μ are quoted to illustrate the sensitivity of the search and quantify the expected distribution of possible outcomes.

Combined Tevatron Higgs search results use the Bayesian technique to quote limits and cross section measurements, and the Frequentist $1 - \mathrm{CL_b}$ p-value to quantify the significance of a signal. The values of LLR are displayed along with their expected distributions to also quantify the data's preference for either the signal-plus-background or the background-only predictions.

4. Searches for the Standard Model Higgs Boson

An early search for the SM Higgs boson[98] was performed by the CDF Collaboration using 91 pb^{-1} of data recorded at $\sqrt{s} = 1.8$ TeV during Run I of the Tevatron Collider. This search considered the associated production mode of a Higgs boson with a hadronically-decaying W or Z boson, with $H \to b\bar{b}$. The low available integrated luminosity and the small total selection efficiency achieved of $\approx$ 1–2%, mainly driven by the limited trigger and double b-tagging efficiency, resulted in a cross section limit that was about two orders of magnitude larger than the SM prediction for a Higgs boson with mass in the 70–140 GeV range.

A broad and competitive program of searches for the SM Higgs boson had to wait until Run II, exploiting much improved detectors and reconstruction algorithms, as well as a factor of ≈ 100 times larger integrated luminosity. Eventually, with 10 fb^{-1} of data analyzed per experiment at $\sqrt{s} = 1.96$ TeV, the combination of searches by the CDF and DØ Collaborations was expected to achieve 95% C.L. exclusion sensitivity to a Higgs boson with mass in the range between 90 GeV and 185 GeV. In the following sections we review the search strategies followed by the Tevatron experiments to achieve this goal, as well as discuss the main characteristics and results of the search channels considered. Then we summarize the final results on the SM Higgs boson from the combination of all available searches, which constitute one of the main legacies of the Tevatron physics program.

4.1. *Search strategies*

The main search modes at the Tevatron in the low m_H region ($\approx$ 90–120 GeV) involve the associated production of a W and Z with a Higgs boson, with the W and Z boson decaying leptonically and $H \to b\bar{b}$. At higher mass ($\approx$ 130–185 GeV), the main search mode is gluon-gluon fusion ($gg \to H$), with $H \to WW^{(*)}$, again involving leptonic W boson decays. For $m_H \sim 125$ GeV, searches for $H \to b\bar{b}$ and $H \to WW^{(*)}$ have comparable sensitivity. Although the above represent the main search channels, other combinations of production and decay modes have also been considered in order to further improve the sensitivity as well as the model-independence of the search. In particular, in the low mass region, decay modes such as $H \to ZZ^{(*)}$, $\tau^+\tau^-$ and $\gamma\gamma$ have also been exploited.

Just considering the main search channels, $\approx$ 40–70 Higgs boson events (assuming m_H in the range of 110–160 GeV) are expected to be produced per experiment and per fb^{-1}, adding up to an expected sample of about 1000 Higgs bosons produced over the complete Run II data set. Selecting and identifying the signal candi-

date events from the overwhelming background represents a major challenge. This resulted in an aggressive program of improvements by the CDF and DØ Collaborations leading to the development of some of the most sophisticated analyses up until now. For every Higgs boson search, the basic strategy involves: (a) selection of the candidate sample, trying to maintain the highest possible acceptance; (b) classification of events into separate categories with different signal-to-background ratio; (c) validation of background predictions in dedicated data control samples; (d) for each category, construction of a variable that is a function of the measured quantities for each event that has the most discrimination between the signal and background, typically involving the use of an MVA discriminant; and (e) test of hypothesis involving the combination of all event categories, including in situ constraints on the dominant systematic uncertainties using high-statistics data control samples.

4.2. *Signal and background modeling*

The modeling of Higgs boson production is performed via leading-order (LO) MC simulations provided by PYTHIA[99] using the LO CTE5L or CTEQ6L1[45,100] PDF sets. While this provides a sufficiently accurate model of the kinematics of Higgs boson production for most processes, further accuracy is sought in modeling the p_{T} spectrum of Higgs bosons produced in the gluon-gluon fusion process. Monte Carlo signal events in this process are reweighted in order match the prediction of the p_{T} distribution predicted at NLO+NNLL accuracy by the HQT program.[35] The decay of the Higgs boson is modeled by PYTHIA with branching ratios predictions from Ref. 48. All MC samples are normalized to the highest-order (NLO or higher) cross section calculation available for the corresponding production process (see Sec. 2).

Higgs boson searches at the Tevatron are affected by large backgrounds that can be categorized as "physics" and "instrumental" backgrounds. The optimized event selections used in the Higgs boson searches often result in the former dominating over the latter. The main physics backgrounds involve the production of a vector boson produced in association with jets (W/Z+jets), single and pair production of top quarks, and diboson (WW, WZ, ZZ) production. Backgrounds from W/Z+jets are typically simulated using MC matrix element generators such as ALPGEN,[101] allowing the simulation of high parton multiplicities at LO. This includes the generation of samples with extra heavy-flavor quarks, such as $W/Zb\bar{b}$+jets and $W/Zc\bar{c}$+jets. These samples are interfaced with PYTHIA for further showering and hadronization, and implement the MLM parton-jet matching algorithm[102] to avoid double-counting of radiation between the matrix-element calculation and the parton shower. Backgrounds from top quark pair production are modeled using PYTHIA (CDF) or ALPGEN+PYTHIA (DØ), while backgrounds from single top quark production are modeled using the MADEVENT[103] (CDF) or SINGLETOP[104] (DØ) event generators, both interfaced to PYTHIA. Finally, diboson production is modeled with PYTHIA. The corresponding MC samples are normalized to higher-order theoretical

cross sections (typically at NLO or higher). In the case of W/Z+jets events, imperfections in the modeling of the vector boson p_{T} or jet kinematics, or the heavy-flavor content, are corrected using data control samples.

Instrumental backgrounds are estimated either entirely from data or by applying data-driven corrections to dedicated MC samples. Examples of instrumental backgrounds include QCD multijet production with jets misidentified as isolated leptons and/or jet energy mismeasurements generating spurious $\not\!\!E_{\mathrm{T}}$. Other examples include $W+\gamma$/jets production with photons and jets misidentified as leptons or $Z/\gamma^*(\to \ell^+\ell^-)$+jets production with fake $\not\!\!E_{\mathrm{T}}$ because of jet energy or lepton momentum mismeasurements. Some searches requiring same-charge leptons are also sensitive to lepton charge mismeasurements, which the simulation programs often do not predict accurately enough and need to be corrected based on measurements in data control samples.

All MC samples are processed through GEANT[105] simulations of the detectors and reconstructed using the same software as used for collision data. The effects from electronic noise and additional proton-antiproton interactions are included either via the simulation (CDF) or by overlaying data events from randomly selected beam crossings on the MC events, in both cases attempting to reproduce the instantaneous luminosity spectrum of the analyzed dataset. Averaging over the entire Run II data sample, approximately two additional proton-antiproton interactions per event were present, which did not result in a significant degradation of the performance of reconstruction algorithms. This is contrast with the average of ≈ 20 proton-proton interactions per crossing recorded by the ATLAS and CMS experiments during the run in 2012 at $\sqrt{s} = 8$ TeV.

4.3. *Searches for $H \to b\bar{b}$*

Searches for $H \to b\bar{b}$ at the Tevatron dominate the sensitivity in the low m_H region ($\approx$ 90–120 GeV), capitalizing on the VH production modes with leptonic W and Z decays, which facilitate event triggering and identification. The main search channels exploited are $WH \to \ell\nu b\bar{b}$, $ZH \to \ell^+\ell^- b\bar{b}$ and $ZH \to \nu\nu b\bar{b}$. While identifying a data sample enriched in W/Z+jets is straightforward using W and Z decays into electrons or muons, it is more challenging in the case of $Z(\to \nu\nu)$+jets owing to the large background from QCD multijet production in such jets+$\not\!\!E_{\mathrm{T}}$ signature. Nevertheless, sophisticated techniques have been developed that allow the effective suppression of the QCD background, making $ZH \to \nu\nu b\bar{b}$ one of the most sensitive search channels in the $H \to b\bar{b}$ decay mode.

The main backgrounds to $VH(\to b\bar{b})$ searches are W/Z+jets and $t\bar{t}$ production. Smaller backgrounds originate from single top, QCD multijet and diboson production. A key experimental handle to suppress the background is the requirement of having at least one b-tagged jet. Over the years, sophisticated MVA b-tagging algorithms have been developed by the CDF and DØ Collaborations (see Sec. 3.3). The b-tagging information can most optimally be used by categorizing events according

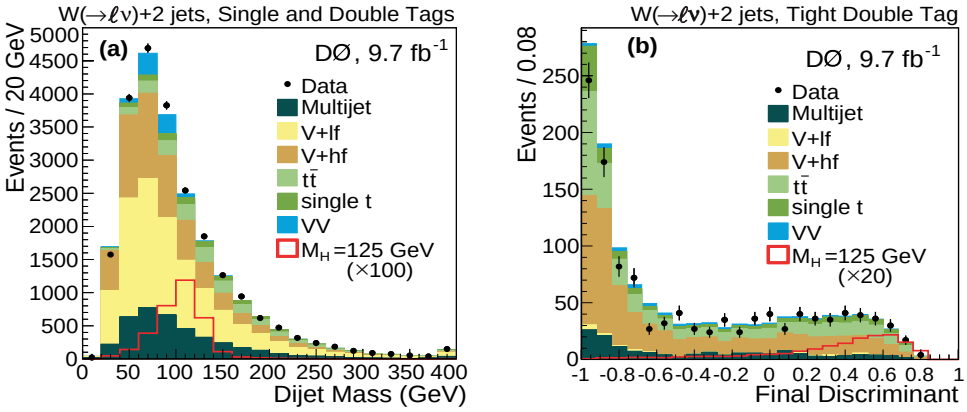

Fig. 2. (a) Distribution of the dijet invariant mass for all b-tag categories combined in the 2-jet channel of the DØ $WH \to \ell\nu b\bar{b}$ search. The data (points with error bars) are compared to the background prediction, broken down into its individual components. Also shown is the expected contribution from a SM Higgs boson with $m_H = 125$ GeV scaled by a factor of 100. (b) Distribution of the final BDT distribution for the tight double b-tag category in the 2-jet channel of the DØ $WH \to \ell\nu b\bar{b}$ search. The data (points with error bars) are compared to the background prediction, broken down into its individual components. Also shown is the expected contribution from a SM Higgs boson with $m_H = 125$ GeV scaled by a factor of 20. From Ref. 106.

to the purity and number of b-tagged jets. Samples with more stringent b-tagging requirements are dominated by V+heavy-flavor jets, and in particular $Vb\bar{b}$, which constitutes an irreducible background. The main discriminating variable between the VH signal and the backgrounds is the dijet invariant mass distribution, which shows a resonant structure around the Higgs boson mass for signal, while it has a smoothly-falling spectrum for background. Therefore, significant efforts have been undertaken to improve the dijet mass resolution (see e.g. Ref. 80). The final step for these searches is to combine a number of kinematic variables into MVA discriminants in order to maximize the sensitivity. A crucial validation of the overall search strategy is provided by the precise measurement of small-cross section backgrounds with the same signature as the signal, such as single top quark and diboson production. Lower-sensitivity searches have also been carried out in the VH and VBF production modes with fully-hadronic final states, as well as in the $t\bar{t}H$ production mode. A summary of the main features and results for all $H \to b\bar{b}$ searches is provided below.

4.3.1. $WH \to \ell\nu b\bar{b}$

The CDF and DØ Collaborations have performed searches for $WH \to \ell\nu b\bar{b}$ using the full Run II dataset.[106–108] These searches have much in common with the single top quark searches and subsequent observations and measurements made previously.[93,109–111] Specifically, since the final state contains the same particle content,

the backgrounds to both analyses are from the same processes, though the signals have different kinematic properties. The single top quark signal has a higher production cross section and more distinct kinematic properties; the fact that the top quark mass was known precisely also helped. The techniques for search and discovery such as background estimation, cut and MVA optimization, and systematic uncertainty estimation were tested, improved, and validated first in the search for single top quarks and then refined for the Higgs boson analyses. Interestingly, many of the improvements made in the Higgs boson searches, such as the more sophisticated b-taggers, were then propagated back into the final single top results.[112–118]

Candidate events are selected requiring a single isolated lepton (e or μ), large $\not\!\!E_T$ and two or three jets in the event, at least one of which is required to be b-tagged. Lepton selections are kept as loose as possible in order to maximize acceptance, requiring the development of sophisticated techniques to suppress the QCD multijet background, leaving a sample dominated by background events containing real leptonic W decays. In both the CDF and DØ analyses, events are categorized into different channels depending on the jet multiplicity (2 or 3 jets) and the number and purity ("loose" (L) or "tight" (T)) of b-tagged jets. As a result, the CDF analysis considers five b-tagging categories (TT, TL, LL, T, L) for the 2-jet sample and two categories (TT, TL) for the 3-jet sample, while the DØ analysis considers four categories (TT, TL, LL, T) and two categories (LL, T), respectively. Channels with two b-tagged jets are enriched in $Wb\bar{b}$, $t\bar{t}$ and single top backgrounds, while channels with one b-tagged jet are dominated by W+light or charm jets, and contain also sizable QCD multijet contributions. For each of the analysis channels, optimized MVA discriminants are trained against the corresponding backgrounds, considering a number of kinematic distributions, in addition to the dijet mass. Figure 2 shows examples of the inclusive dijet mass distribution (summed over all analysis channels) and the final MVA discriminant in the most sensitive channel of the DØ search. The observed (expected) cross section limits at $m_H = 125$ GeV for the CDF and DØ analyses are 4.9 (2.8) and 5.2 (4.7) times the SM prediction, respectively.

4.3.2. $ZH \to \ell^+\ell^- b\bar{b}$

The CDF and DØ Collaborations have performed searches for $ZH \to \ell^+\ell^- b\bar{b}$ using the full Run II dataset.[119–121] Candidate events are selected requiring two opposite-sign (OS) same-flavor isolated leptons (e^+e^- or $\mu^+\mu^-$) and two or three jets in the event, at least one of which is required to be b-tagged. Lepton selections are kept as efficient as possible in order to maximize acceptance, since after the requirement that the two leptons form a Z boson candidate, background from misidentified leptons is negligible. In any case, events are categorized according to the quality of the identified leptons. Similarly to the WH analysis, different event categories are defined based on jet and b-tag multiplicities, and on b-tag purity requirements. The CDF analysis considers four b-tagging categories (TT, TL, LL, T) for both the 2-jet and 3-jet samples, while the DØ analysis considers two categories (TL, T) for

both the 2-jet and 3-jet samples. The absence of $\not\!\!E_T$ in the event allows for improved invariant mass resolution by imposing event-wide transverse momentum constraints: in the case of the CDF analysis corrections to the jet energies are performed via a dedicated NN relating the measured jet energies and directions to the $\not\!\!E_T$ vector on an event-by-event basis; in the case of the DØ analysis an improved measurement of the jet energy is obtained from a kinematic fit imposing constraints on the dilepton mass to be consistent with the Z boson mass and that the missing transverse momentum of the leptons-plus-jets system should be consistent with zero. A sophisticated MVA strategy is followed whereby different MVA discriminants are trained to separate the signal from the different backgrounds (Z+jets, $t\bar{t}$ and diboson), one at a time. The observed (expected) cross section limits at $m_H = 125$ GeV for the CDF and DØ analyses are 7.1 (3.9) and 7.1 (5.1) times the SM prediction, respectively.

4.3.3. $WH, ZH \to \not\!\!E_T b\bar{b}$

The CDF and DØ Collaborations have performed searches for $ZH \to \nu\nu b\bar{b}$ using the full Run II dataset.[85,122,123] Candidate events are selected requiring at least two jets (CDF) or exactly two jets (DØ), no identified leptons and significant $\not\!\!E_T$ not aligned with the jet directions. Dedicated triggers using $\not\!\!E_T$ are used with or without accompanying jets. About half of the signal events in this channel originate from $WH \to \ell\nu b\bar{b}$ with the charged lepton not identified, hence the name $WH, ZH \to \not\!\!E_T b\bar{b}$ given to this search. As the previous $VH(\to b\bar{b})$ searches, different event categories are defined based on b-tag multiplicity and purity requirements: the CDF analysis considers three b-tagging categories (TT, TL, T), while the DØ analysis considers two categories which are defined by requirements on the sum of the b-tagging output variables for the two taggable jets in the event. The large QCD multijet background with spurious $\not\!\!E_T$ is effectively suppressed via MVA discriminants that exploit information of the $\not\!\!E_T$ as measured by the calorimeter and by the tracker, including the correlation between their directions in the transverse plane and with respect to the directions of the jets. As a result, after final selection the QCD multijet background can be made comparable or significantly smaller than the physics background, dominated by V+heavy-flavor and $t\bar{t}$. For each of the analyzed samples, MVA discriminants are trained between the signal and all backgrounds. The observed (expected) cross section limits at $m_H = 125$ GeV for the CDF and DØ analyses are 3.1 (3.3) and 4.3 (3.9) times the SM prediction, respectively.

4.3.4. $VH(\to b\bar{b})$ *search results and validation*

The CDF and DØ Collaborations have performed individual combinations of their $VH(\to b\bar{b})$ search results. The CDF combined search[124] excludes a SM Higgs boson with a mass in the range of 90–96 GeV and finds a broad excess with smallest local p-value at a mass of 125 GeV corresponding to a significance of 2.7 s.d. In the case of the DØ combination,[125] the excluded mass range is 100–102 GeV and

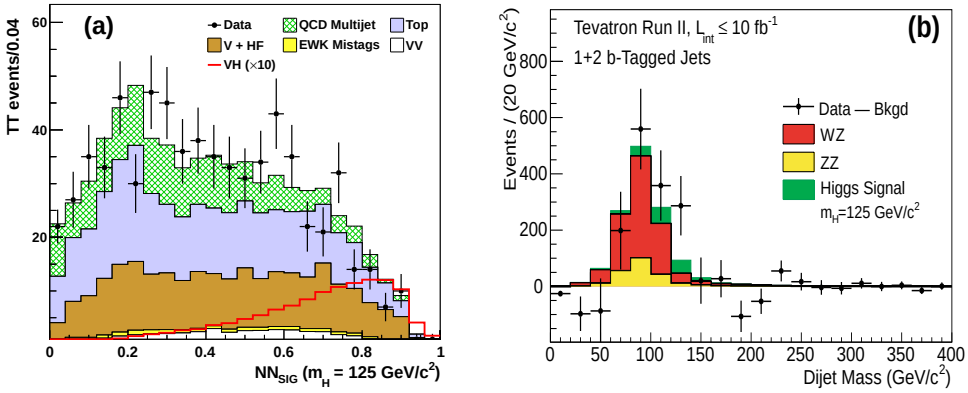

Fig. 3. (a) Distribution of the final NN discriminant for the TT category of the CDF $WH, ZH \to \not\!\!E_T\, b\bar{b}$ search (see text for details). The data (points with error bars) are compared to the background prediction, broken down into its individual components. Also shown is the expected contribution from a SM Higgs boson with $m_H = 125$ GeV scaled by a factor of 10. Adapted from Ref. 123. (b) Background-subtracted distribution of the reconstructed dijet mass, summed over all CDF and DØ channels contributing to the VZ analysis. The fitted VZ and the expected SM Higgs (assuming $m_H = 125$ GeV) contributions are shown with filled histograms. From Ref. 13.

the smallest local p-value is found at a mass of 135 GeV and corresponds to a significance of 1.7 s.d. The combined result from both experiments[12] reached a maximum local significance of 3.3 s.d. at a mass of 135 GeV, becoming 3.1 s.d. after taking into account the LEE, thus representing the first evidence for the presence of a particle produced in association with a W or Z boson and decaying to $b\bar{b}$. Since then, the CDF $WH, ZH \to \not\!\!E_T b\bar{b}$ result was updated[123] to use a more powerful MVA b-tagging algorithm along with changes in the kinematic selections, resulting in a statistical fluctuation that slightly reduced the significance of the excess. The measured combined cross section times branching ratio at $m_H = 125$ GeV from the updated combination[13] is $(\sigma_{WH} + \sigma_{ZH}) \times \mathcal{B}(H \to b\bar{b}) = 0.19^{+0.08}_{-0.09}$ (stat + syst) pb, about 1.5 times larger than the SM prediction at the same mass. Results from the combination of $H \to b\bar{b}$ searches with the rest of search channels are provided in Sec. 4.8.

The sophisticated analysis techniques and methodology used in the $VH(\to b\bar{b})$ searches are validated by measuring the cross section for VZ production, with the Z boson decaying into heavy-flavor jets. This process has the same signature as the signals of interest, including the feature of a resonance in the $b\bar{b}$ invariant mass spectrum. While the SM prediction for the cross section for $VZ(\to b\bar{b})$ is about six times larger than for the Higgs boson signal, this process is affected by larger background from V+jets owing to the lower invariant mass of the $b\bar{b}$ system compared to the VH signal. Exactly the same analyses as for the Higgs boson search are used for this measurement, with the only difference being that MVA discriminants are

trained considering VZ as the signal of interest, and potential contributions from Higgs boson production are not considered. The measured cross section from the combination of CDF and DØ analyses[13] is $\sigma_{VZ} = 3.0 \pm 0.6$ (stat.) ± 0.7 (syst.) pb, in good agreement with SM prediction of 4.4 ± 0.3 pb.[126] Individual measurements by the CDF and DØ Collaborations[127,128] are also found to be consistent with the SM prediction. Figure 3(b) shows the combined background-subtracted dijet invariant mass distribution, clearly showing an excess compatible in yield and shape with that expected from VZ.

4.3.5. $VH, q\bar{q}H \to jjb\bar{b}$

The CDF Collaboration has performed a search for $H \to b\bar{b}$ in the fully-hadronic final state using 9.45 fb^{-1} of data.[129] This search focuses on the VH and VBF production modes resulting in a signature consisting of four or five jets, at least two of which are b-tagged. Two different b-tagging algorithms with different efficiency and purity are employed, and different analysis channels are defined based on the algorithms contributing to each b-tagged jet. The main background originates from QCD multijet production and is modeled directly from data. Multivariate discriminant variables are constructed in each of the analyzed channels to separate the signal from the background. The observed (expected) cross section limit at $m_H = 125$ GeV is 9.0 (11.0) times the SM prediction.

4.3.6. $t\bar{t}H \to t\bar{t}b\bar{b}$

The CDF Collaboration has performed a search for $t\bar{t}H \to t\bar{t}b\bar{b}$ in the lepton-plus-jets final state using 9.45 fb^{-1} of data.[130] Events are selected requiring one electron or muon, large $\not\!\!E_T$ and at least four jets. Similarly to the $VH, q\bar{q}H \to jjb\bar{b}$ search, two different b-tagging algorithms with different efficiency and purity are employed. Events are categorized into different channels depending on their jet multiplicity (4, 5 and ≥ 6 jets), the number of b-tags and the algorithms contributing to each b-tagged jet. Multivariate discriminant variables are constructed in each of the analyzed channels to separate the signal from the dominant $t\bar{t}$+jets background. The observed (expected) cross section limit at $m_H = 125$ GeV is 20.5 (12.6) times the SM prediction. The DØ Collaboration has also performed a search for $t\bar{t}H \to t\bar{t}b\bar{b}$ using 2.1 fb^{-1} of data,[131] with an observed (expected) limit of 84.8 (64.2) times the SM prediction; this result is not included in the combination.

4.4. *Searches for $H \to \tau^+\tau^-$*

The CDF and DØ Collaborations have performed a number of searches involving hadronic τ leptons (τ_h) attempting to probe the $H \to \tau^+\tau^-$ decay mode. Searches for $H+X \to \ell\tau_h$+jets are sensitive to the main Higgs boson production mechanisms, $gg \to H$, VH and VBF, and to both $H \to WW^{(*)}$ and $H \to \tau^+\tau^-$ decays. The DØ search[132] uses 9.7 fb^{-1} of data and requires an electron or muon, a τ_h and at least two

jets, while the CDF search,[133] which uses 6 fb^{-1} of data, considers in addition events with exactly one jet. The dominant backgrounds in these searches originate from W/Z+jets, $t\bar{t}$ and QCD multijet backgrounds. Multivariate techniques are employed to separate signal from background by making use of a large number of kinematic variables. In the case of the DØ analysis, a BDT trained to distinguish between $H \to \tau^+\tau^-$ and $H \to WW^{(*)}$ signals is used to define $\tau\tau$- and WW-dominated samples, which are analyzed separately for decay mode-specific limits, or in combination assuming the SM prediction for the ratio of $H \to \tau^+\tau^-$ and $H \to WW^{(*)}$ branching ratios. The most restrictive limit for the $H \to \tau^+\tau^-$ decay mode is obtained by the DØ $\tau\tau$-specific discriminant, yielding an observed (expected) cross section limit at $m_H = 125$ GeV of 12.8 (10.4) times the SM prediction. The observed (expected) cross section limit obtained by the CDF Collaboration is 16.4 (16.9) times the SM prediction, but it does not correspond specifically to the $H \to \tau^+\tau^-$ decay mode, as it also includes a non-negligible contribution from $H \to WW^{(*)}$ decays. Additional sensitivity to the $H \to \tau^+\tau^-$ decay mode is achieved via searches probing the VH production mechanism together with $H \to \tau^+\tau^+$, leading to trilepton final states ($ee\mu$, $e\mu\mu$ and $\mu\tau_h\tau_h$) involving both leptonic and hadronic τ decays.[134,135]

4.5. *Searches for $H \to WW^{(*)}$*

While searches for $H \to WW^{(*)}$ typically reach their highest sensitivity at the maximum of $\sigma_H \times \mathcal{B}(H \to WW^{(*)})$ as a function of m_H, around $m_H = 165$ GeV, these searches significantly contribute to the combined sensitivity down to $m_H \sim 125$ GeV. A number of searches have been developed targeting different Higgs boson production and decay modes, resulting in very different topologies, depending on the number of charged leptons, whether they have the same or opposite charge, and the number of additional jets considered. The most sensitive topology involves a pair of OS charged leptons and no additional jets, aiming at isolating the $gg \to H \to WW^{(*)} \to \ell^+\nu\ell^-\bar{\nu}$ signal. Searches for OS dileptons are dominated by e^+e^-, $\mu^+\mu^-$ and $e^\pm\mu^\mp$ but final states with one τ_h, $e\tau_h$ and $\mu\tau_h$, have also been considered. Other searches require two same-sign (SS) charged leptons or three leptons (trileptons), being primarily sensitive to the VH production mode, with $H \to WW^{(*)}$. More challenging searches exploiting the semileptonic decay mode of the $WW^{(*)}$ pair, $H \to WW^{(*)} \to \ell\nu q\bar{q}'$, have also been developed. A summary of the main features and results for these searches is provided below.

4.5.1. *Opposite-sign dileptons*

The CDF and DØ Collaborations have searched for $H \to WW^{(*)}$ with both W bosons decaying leptonically, giving an experimentally clean signature of two OS charged leptons (e or μ) and significant $\not\!\!E_T$.[134,136] These searches are sensitive to the three main Higgs boson production mechanisms, although $gg \to H$ dominates the sensitivity. Since at low m_H one of the W bosons from the Higgs boson decay

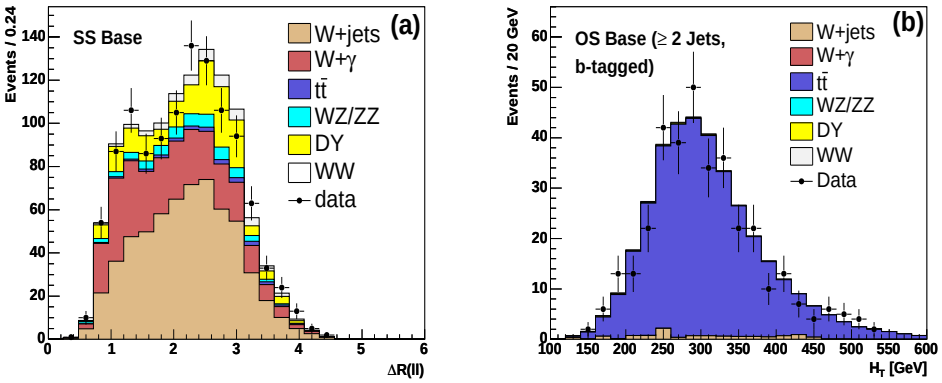

Fig. 4. (a) Distribution of the three-dimensional angular separation between the two charged leptons ($\Delta R(\ell^+, \ell^-)$) in the SS dilepton+0, 1 jets control sample used to validate the modeling of W+jets/γ backgrounds in the CDF $H \to WW^{(*)}$ search. From Ref. 136. (b) Distribution of the scalar sum of the lepton $p_{\rm T}$, $\not\!\!E_T$ and $p_{\rm T}$ of the jets ($H_{\rm T}$) in the OS dilepton+$\geq$ 2 jets/$\geq$ 1 b-tags control sample used to validate the modeling of the $t\bar{t}$ background in the CDF $H \to WW^{(*)}$ search. The data (points with error bars) are compared to the background prediction, broken down into its individual components. From Ref. 136.

is off-shell, lepton selections optimized down to low $p_{\rm T}$ have been developed. After $\not\!\!E_T$ requirements, the main backgrounds are non-resonant W^+W^- with two real leptons, and W+jets and $W+\gamma$ with a jet or photon mimicking the signature of an isolated lepton. Additional contributions, primarily affecting the same-flavor dilepton channels (ee and $\mu\mu$) originate from Z/γ^*+jets with jet energy mismeasurements causing spurious $\not\!\!E_T$. At higher jet multiplicity, the contribution from dileptonic $t\bar{t}$ events can be substantial even after vetoing b-tagged jets. Finally, smaller background contributions arise from WZ and ZZ processes. Backgrounds are estimated using a combination of MC simulations and data-driven techniques. In the case of backgrounds with real leptons and true $\not\!\!E_T$ from neutrinos, the MC simulation is used. On the other hand, instrumental backgrounds originating from the misidentification of jets or photons as leptons (W+jets/γ) or mismeasured $\not\!\!E_T$ (Z/γ^*+jets), are not sufficiently well modeled by the simulation, which is improved by applying dedicated data-based corrections. Detailed comparisons between the data and the background predictions are made in dedicated control samples enriched in one background at a time (see examples in Fig. 4).

In contrast with $H \to b\bar{b}$ searches, in the case of $H \to WW^{(*)}$ the presence of two neutrinos in the final state precludes the reconstruction of the Higgs boson mass, therefore other discriminating variables against the backgrounds are used. One of the most sensitive kinematic variables is the angular separation between the two charged leptons, either in two dimensions ($\Delta\phi(\ell^+, \ell^-)$) or three dimensions ($\Delta R(\ell^+, \ell^-)$), since the spin-zero nature of the Higgs boson causes the leptons to

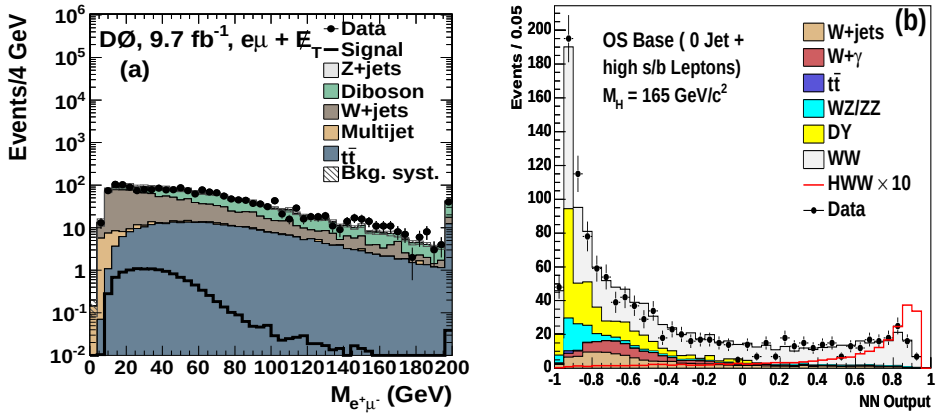

Fig. 5. (a) Distribution of the dilepton invariant mass in the $e^{\pm}\mu^{\mp} + \not\!\!E_T$ channel from the DØ $H \to WW^{(*)}$ search. The data (points with error bars) are compared to the background prediction, broken down into its individual components. Also shown is the expected contribution from a SM Higgs boson with $m_H = 125$ GeV. From Ref. 134. (b) Distribution of the neural network output variable in the OS/0-jet/high s/b channel from the CDF $H \to WW^{(*)}$ search. The data (points with error bars) are compared to the background prediction, broken down into its individual components. Also shown is the expected contribution from a SM Higgs boson with $m_H = 125$ GeV scaled by a factor of 10. From Ref. 136.

be produced closer to each other on average than is the case for the background. For the same reason, the dilepton invariant mass distribution shows good discrimination between signal and background (see Fig. 5(a)). In order to optimize the search sensitivity, events are categorized into different analysis channels with different signal-to-background ratio and background composition, and optimized MVA discriminants are defined and trained for each of them. Both CDF and DØ categorize events according to the number of jets, with the 0-jet channel primarily probing the $gg \to H$ production mechanism and the 1-jet and 2-jet channels being more sensitive to VH and VBF production. Categories are also defined based on the lepton quality (CDF) or lepton flavor (DØ). An example of the MVA discriminant for the single highest-sensitivity channel in the CDF analysis, requiring exactly 0 jets and high-purity leptons, is shown in Fig. 5(b), demonstrating the good separation between signal and background achieved. The DØ analysis further categorizes events with exactly 0 or 1 jets according to an MVA discriminant designed to separate WW-like events (including both $H \to WW^{(*)}$ signal and non-resonant WW background) from non-WW events. The CDF analysis also considers a separate channel for events with dilepton invariant mass below 16 GeV. Finally, searches for $H \to WW^{(*)} \to e\tau_h, \mu\tau_h + \leq 1$ jets have also been performed.[132,134]

4.5.2. *Same-sign dileptons and trileptons*

The CDF and DØ Collaborations have performed a number of searches for VH production in association with $H \to WW^{(*)}$, involving two or more leptonic W or Z decays.[134,135] The resulting signatures include SS dileptons-plus-jets, e.g. from $W^{\pm}H \to W^{\pm}W^{+}W^{-} \to \ell^{\pm}\nu\ell^{\pm}\nu jj$, and trileptons, e.g. from $W^{+}H \to W^{+}W^{+}W^{-} \to \ell^{+}\nu\ell^{+}\nu\ell^{-}\nu$ or $ZH \to ZW^{+}W^{-} \to \ell^{+}\ell^{-}\nu\ell^{+}\nu jj$. While SS dilepton analyses only consider electrons and muons, some trilepton analyses allow for up to one τ_h. These searches are characterized by small expected signal contributions, but also small backgrounds, dominated by V+jets/γ with jets or photons misidentified as leptons, and diboson (WZ, ZZ) production. Multiple analysis channels are defined, depending on the lepton flavor, the jet multiplicity, and whether a dilepton pair has mass close to M_Z in the trilepton channels. MVA discriminants are constructed for each of them making use of several kinematic variables, among which the event $\not\!\!E_T$ is found to be particularly useful, owing to the presence of multiple neutrinos in the signal as compared to the main background processes.

4.5.3. *Lepton-plus-jets*

The DØ Collaboration has performed a search for $H \to WW^{(*)} \to \ell\nu q\bar{q}'$ using the full Run II dataset.[108] This search considers events with exactly one electron or muon, large $\not\!\!E_T$ and at least two jets, requiring either that there are no b-tagged jets or at the most there is exactly one b-tagged of the lowest purity that can originate from a c quark. This ensures a non-overlapping selection with that used in the $WH \to \ell\nu b\bar{b}$ search. Events are further categorized according to their lepton flavor (e or μ), their jet multiplicity (2 jets, 3 jets or ≥ 4 jets) and the number of b-tagged jets. The selections with 2 or 3 jets are primarily sensitive to the $gg \to H$ production mode, while the selection with ≥ 4 jets targets the associated production mode, $VH \to \ell\nu q\bar{q}'q\bar{q}'$. Multivariate discriminants are trained to separate signal from the overwhelming W+jets background. The best expected sensitivity for these searches is achieved at $m_H = 165$ GeV, reaching 4.0 and 7.3 times the SM Higgs boson cross section for the 2+3-jet channels and ≥ 4 jets channel, respectively. The corresponding observed limits are 2.8 and 8.5 times the SM prediction, respectively.

4.5.4. $H \to WW^{(*)}$ *search results and validation*

The combination of CDF and DØ searches for $H \to WW^{(*)}$ using only 4.8–5.4 fb^{-1} of data[137] reached 95% C.L. exclusion of a SM Higgs boson with mass in the range of 162–166 GeV, the first exclusion above the LEP limit. After analyzing the full Run II dataset and substantially improving the analyses, each experiment has been able to exclude a substantial mass range: 149–172 GeV and 157–172 GeV in case of the CDF and DØ combinations, respectively. The expected sensitivities reached at a mass of 125 GeV are 3.1 and 3.0 times the SM Higgs boson cross section for the CDF and DØ searches, respectively. More details on the expected and observed

sensitivities, as well as the combination of searches, are provided in Sec. 4.8.

Once again, the measurement of diboson cross sections using the same experimental techniques as for the $H \to WW^{(*)}$ searches, provides an important validation of the search methodology. Both collaborations have performed measurements of the W^+W^- cross section in the $\ell^+\nu\ell^-\bar{\nu}$ final state,[136,138] the ZZ cross section in the $\ell^+\ell^-\nu\bar{\nu}$ final state,[139,140] and the WZ cross section in the $\ell^+\nu\ell^+\ell^-$ final state,[140,141] finding good agreement with NLO predictions.

4.6. *Searches for* $H \to ZZ^{(*)}$

The CDF and DØ Collaborations have performed searches for $H \to ZZ^{(*)} \to \ell^+\ell^-\ell'^+\ell'^-$ $(\ell, \ell' = e, \mu)$ using the full Run II dataset.[142,143] While this channel constitutes a discovery mode at the LHC, at the Tevatron the exceedingly small branching ratio for $H \to ZZ^{(*)} \to 4\ell$, coupled with the limited integrated luminosity available, results in a small expected sensitivity. These searches are characterized by very small expected signal, but also small backgrounds from non-resonant production of $(Z/\gamma^*)(Z/\gamma^*)$. In order to maximize the signal acceptance, these searches select leptons with p_{T} down to 10 GeV and relaxed lepton identification criteria. The four-lepton invariant mass distribution constitutes the most discriminating variable to separate $gg \to H \to ZZ^{(*)}$ from the background. In addition, the event $\not\!\!E_{\mathrm{T}}$ is employed to increase the sensitivity to signal contributions from $ZH \to ZW^+W^+ \to \ell^+\ell^-\ell^+\nu\ell^-\bar{\nu}$ and $ZH \to \ell^+\ell^-\tau^+\tau^-$, particularly at low m_H. Figure 6(b) shows the four-lepton invariant mass distribution used by the CDF analysis. No excess compatible with a Higgs boson signal is found and the $(Z/\gamma^*)(Z/\gamma^*)$ cross section is measured finding good agreement with the SM prediction.[143,144] The best expected sensitivity is achieved for m_H near 150 GeV and 190 GeV, reaching approximately 10 times the SM prediction. The observed (expected) cross section limits at $m_H = 125$ GeV for the CDF and DØ analyses are 29.3 (26.5) and 42.8 (42.3) times the SM prediction, respectively.

4.7. *Searches for* $H \to \gamma\gamma$

The CDF and DØ Collaborations have performed searches for $H \to \gamma\gamma$ using the full Run II dataset.[142,143] The small $H \to \gamma\gamma$ branching fraction in the SM makes these searches at the Tevatron not promising in terms of sensitivity to the SM Higgs boson, although the large enhancements possible to $\mathcal{B}(H \to \gamma\gamma)$ in beyond-SM scenarios open a window of opportunity that makes them well justified. These searches consider the three main Higgs boson production modes, exploiting their kinematic differences with respect to the main backgrounds, consisting of non-resonant $\gamma\gamma$ production, followed by γ+jets and QCD dijets with one or two jets misidentified as photons. The CDF search selects photon candidates in both the central and forward calorimeters, while the DØ analysis is restricted to photons in the central calorimeter. In both searches, events are classified in categories with different signal-to-background ratio in order to optimize the search sensitivity: the CDF

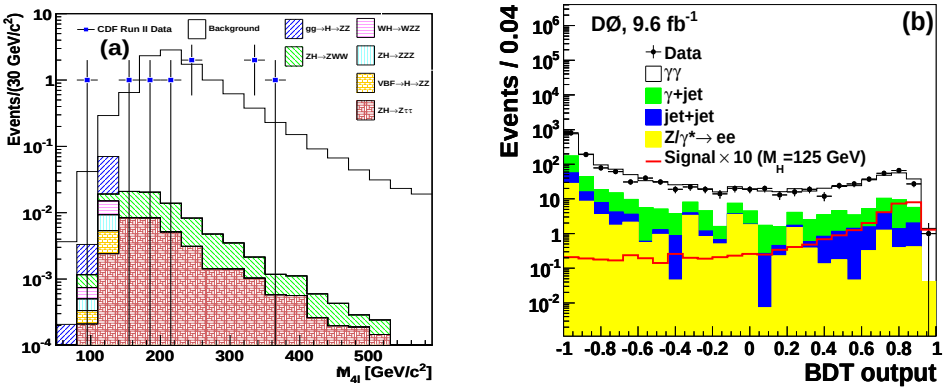

Fig. 6. (a) Distribution of the four-lepton invariant mass used by the CDF $H \to ZZ^{(*)} \to 4\ell$ search. The data (points with error bars) are compared to the total background prediction, shown with an open histogram. Also shown are the expected contributions from a SM Higgs boson with $m_H = 125$ GeV, broken down into several components, shown hatched and stacked. Adapted from Ref. 145. (b) Distribution of the BDT distribution used by the DØ $H \to \gamma\gamma$ search in the photon-enriched sample. The data (points with error bars) are compared to the background prediction, broken down into its individual components. Also shown is the expected contribution from a SM Higgs boson with $m_H = 125$ GeV scaled by a factor of 10. From Ref. 143.

analysis defines up to six different categories (depending on pseudorapidity of the photons and whether or not a photon candidate is identified as originating from a $\gamma \to e^+e^-$ conversion), while the DØ analysis defines two categories (photon-enriched and jet-enriched, depending on the output from an MVA used for photon identification). Both searches construct MVA discriminants exploiting the diphoton mass as well as other kinematic variables to separate the signal from the background. The CDF search applies MVA discriminants only to the highest-sensitivity channels with two central photons, using the diphoton mass in the rest of channels, whereas the DØ uses the MVA discriminants in all analysis channels. Figure 6(b) shows the MVA distribution used by the DØ analysis in the photon-enriched region. These searches have a relatively constant sensitivity as a function of m_H in the range $100 < m_H < 140$ GeV. The observed (expected) cross section limits at $m_H = 125$ GeV for the CDF and DØ analyses are 17.0 (9.9) and 12.8 (8.7) times the SM prediction, respectively.

4.8. *Standard Model Higgs boson search results*

Both the CDF and DØ Collaborations performed searches for the SM Higgs boson in the channels described in Secs. 4.3–4.7. The interaction between the collaborations' analysis teams was minimal when the analyses were developed and optimized. As more data were collected, the results from each channel were combined together to form collaboration-wide results using the statistical methods described in Sec. 3.7,

and the communication between the experiments' analysis teams increased in order to propagate the techniques that were found to be the most sensitive. Each collaboration prepared individual channel results as well as combined results, and the same techniques, described in Sec. 3.7, were used to combine CDF and DØ's results together to produce single results with the maximum sensitivity.

Producing combined results from CDF and DØ's searches required significant coordination between the two collaborations, and thus the Tevatron New Physics and Higgs Working Group (TEVNPHWG) was formed. The combinations needed to preserve all of the statistical power and systematic rigor of the contributing analyses, and thus detailed exchange of data distributions and predictions from each signal and background process was performed. All systematic uncertainties affecting the rates and shapes of the predicted distributions were also exchanged and itemized by source. The list of correlated systematic uncertainties was determined by the two collaborations, accounting for cases where the same predictions and uncertainties were shared by both. Recommendations from the TEVNPHWG for central values and uncertainties for shared sources of systematic uncertainty were propagated to the collaborations' analysis teams to unify the treatment and to make the joint fits of data between the two experiments consistent. Frequently, combined results were required to be produced for the same conference as the individual contributing results, and so the exchange formats, combination techniques, and systematic uncertainty categories were formalized well in advance. Combinations were always performed twice, once by the CDF group members using the Bayesian method, and once by the DØ group members using the Modified Frequentist method, and results were approved only when consistency was achieved.

4.8.1. *Limits*

During the first years of Run II, the Tevatron experiments were not yet sensitive to the SM Higgs boson at its predicted rate but could set limits on the signal strength modifier μ. Even though physics models do not scale the five mechanisms $gg \to H$, WH, ZH, VBF, and $t\bar{t}H$ together, the expected limit on a common scale factor defined the sensitivity of the searches. If the observed limit on μ falls below unity for a particular m_H, that value of the Higgs boson mass is excluded at the 95% C.L. Figure 7 shows the observed and expected upper limits on μ (labeled "95% CL Limit/SM") as a function of m_H for the full Run II data sample. Values of m_H between 90 GeV and 109 GeV, and also between 149 GeV and 182 GeV, are excluded at the 95% C.L. The expected exclusion regions are between 90 GeV and 120 GeV and also between 140 GeV and 184 GeV, assuming no Higgs boson is present. Excesses are seen in the low-mass searches between m_H values of 115 GeV and 135 GeV, as well as in the high-mass searches (dominated by the $H \to WW^{(*)}$ searches) around $m_H = 200$ GeV. The excess at around $m_H = 200$ GeV is in a region where the sensitivity is not as strong as at lower masses, and where the mass resolution is quite poor. Shown along with the expected limits assuming no Higgs

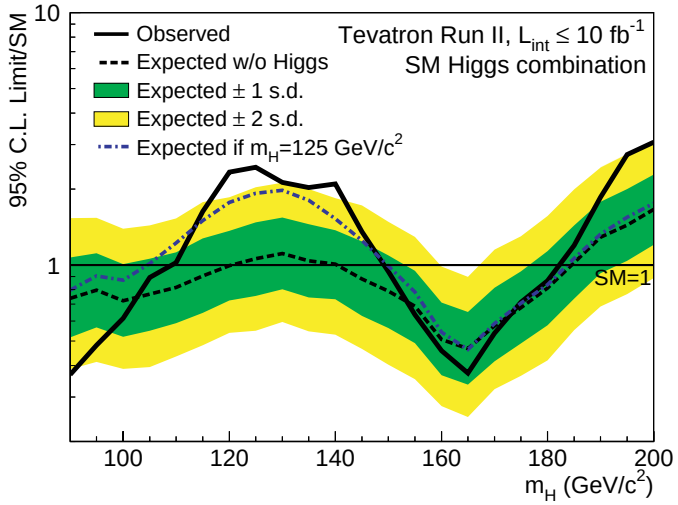

Fig. 7. Observed and median expected (for the background-only hypothesis) 95% C.L. Bayesian upper production limits expressed as multiples of the SM cross section as a function of Higgs boson mass for the combined CDF and DØ searches in all decay modes. The dark- and light-shaded bands indicate, respectively, the one and two standard deviations (s.d.) probability regions in which the limits are expected to fluctuate in the absence of signal. The blue short-dashed line shows median expected limits assuming the SM Higgs boson is present at $m_H = 125$ GeV. From Ref. 13.

boson is present are the expected limits as a function of the test mass assuming a Higgs boson is present at $m_H = 125$ GeV.

4.8.2. *Significance*

To quantify the significance of excess data candidates compared with the background, the background-only p-value 1-$\mathrm{CL_b}$ using LLR as the test statistic is computed. The observed and expected values of LLR are shown as functions of m_H in Fig. 8(a). The expected values are shown for the null hypothesis (SM backgrounds but without a Higgs boson contribution) and the test hypothesis (the SM Higgs boson is present at the m_H being tested), and the 68% and 95% intervals around the null hypothesis's predictions are shown. The expected values assuming the SM Higgs boson is present at $m_H = 125$ GeV are likewise shown.

The signal significance as a function of the tested m_H is shown in Fig. 8(b). It shows the probability of obtaining an LLR value at least as signal-like as the observed value, as a function of m_H, as well as the median expected value of this probability and its expected distribution owing to expected random outcomes if no Higgs boson is present, if a Higgs boson is present at each value of m_H tested, and if a Higgs boson is present at $m_H = 125$ GeV. A local significance of 3.0 standard deviations (s.d.) is observed for $m_H = 125$ GeV, and 1.9 s.d. are expected assuming the SM Higgs boson is present with the SM predicted rate.[13]

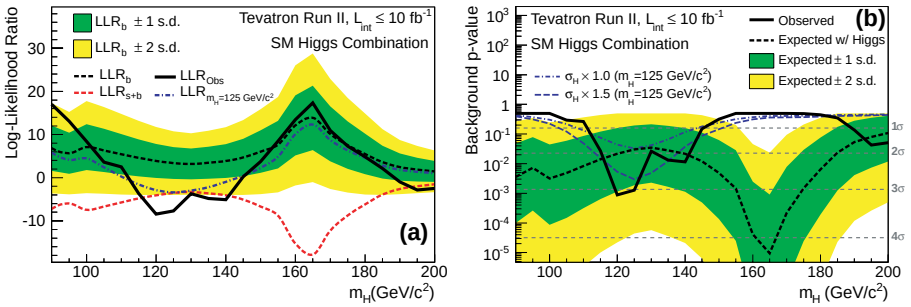

Fig. 8. (a) Log-likelihood ratio (LLR) for the Tevatron's Higgs boson searches in all decay modes combined. The solid line shows the observed LLR as a function of m_H. The median background-only expectation and its expected variation is shown with a dark long-dashed line and shaded bands. The median expectation assuming the SM Higgs boson is present at $m_H = 125$ GeV is shown with a blue dashed line and the median expectation assuming a Higgs boson is present at each value of m_H in turn is shown with a red dashed line. From Ref. 13. (b) The background p-value as a function of m_H is shown with a solid line. The dotted black line shows the median expected values assuming a SM signal is present, evaluated separately at each m_H, and the shaded bands indicate the expected variations. The blue lines show the median expected p-values assuming the SM Higgs boson is present with m_H=125 GeV at signal strengths of 1.0 times (short-dashed) and 1.5 times (long-dashed) the SM prediction. From Ref. 13.

4.8.3. *Cross section fits*

The best-fit value of the signal strength modifier μ is shown as a function of m_H in Fig. 9(a), along with the expectation assuming a Higgs boson is present at $m_H = 125$ GeV, using the Bayesian method described in Sec. 3.7. The 68% and 95% intervals shown along with the cross section fit are the observed credibility intervals and not the expected confidence intervals as shown in the LLR, limit, and p-value plots.

The properties of the excess of candidates seen by the Tevatron experiments are investigated first by measuring the production cross section times the branching ratio in the several decay modes. The searches performed are typically sensitive to one decay mode each, although some searches have contributions from two or more, such as the $H \to WW^{(*)} \to \ell^+\nu\ell^-\bar{\nu}$ searches, which have some acceptance for $H \to \tau^+\tau^-$ events in which the tau leptons decay leptonically. All relevant channels are included in the combination by decay mode in Fig. 9(b).

4.8.4. *Coupling constraints*

A further step in interpreting the excess in the Higgs boson searches at the Tevatron is to test models in which the couplings of the W, Z, or fermions is modified relative to their SM predictions. The prescription of Ref. 146 is followed, where the Higgs boson's couplings to fermions are modified by a multiplicative factor κ_f, to the vector bosons W and Z by κ_V when tested together assuming custodial symmetry, and by κ_W and κ_Z when tested separately. For each value of the κ

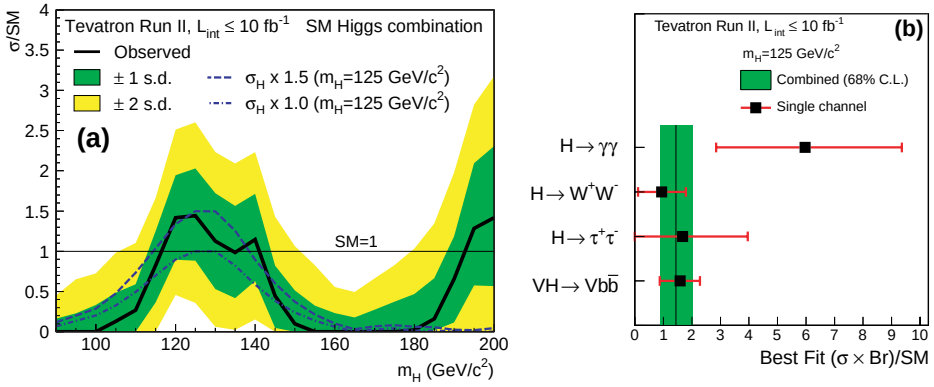

Fig. 9. (a) Best-fit signal cross section expressed as a ratio to the SM cross section as a function of Higgs boson mass for all of CDF and DØ's SM Higgs boson searches in all decay modes combined, assuming SM branching fractions. The dark- and light-shaded bands show the one and two s.d. uncertainty ranges on the fitted signal, respectively. Also shown with blue lines are the median fitted cross sections expected for a SM Higgs boson with $m_H = 125$ GeV at signal strengths of 1.0 times (short-dashed) and 1.5 times (long-dashed) the SM prediction. From Ref. 13. (b) Best-fit values of $\mu = (\sigma \times \mathcal{B})/\mathrm{SM}$ using the Bayesian method for the combinations of CDF and DØ's Higgs boson search channels focusing on the $H \to b\bar{b}$, $H \to \tau^+\tau^-$, $H \to WW^{(*)}$ and $H \to \gamma\gamma$ decay modes for a Higgs boson mass of 125 GeV. The shaded band corresponds to the one s.d. uncertainty on the best-fit value of μ for all SM Higgs boson decay modes combined. From Ref. 13.

coupling modifiers, a new set of Higgs boson production cross sections and branching ratios is computed starting with the SM predictions and modifying each component diagram by the relevant combination of coupling modifiers. For example, the $H \to \gamma\gamma$ width contains a contribution scaled by κ_f due to the top-quark and b-quark loops, and a contribution with the opposite sign in the amplitude coming from the W-boson loop. A uniform prior is assumed in the two-dimensional planes (κ_V, κ_f) and (κ_W, κ_Z), in which the results are shown in Fig. 10. No significant deviations from the SM predictions are seen.

4.8.5. *Tests of spin and parity*

Recent progress has been made at the Tevatron in testing the spin and parity of the Higgs boson using the model predictions of Ref. 147. The threshold behavior of the associated production of a pseudoscalar ($J^P = 0^-$) and a graviton-like ($J^P = 2^+$) exotic higgs boson with a vector boson V (W or Z) differ markedly from those of the SM Higgs boson ($J^P = 0^+$). The SM Higgs associated production is an s-wave process and its cross section rises proportional to β close to threshold, where $\beta = 2p/\sqrt{s}$, with p being the magnitude of the three-momentum of the Higgs boson (or the vector boson) in the VH rest frame, and $\sqrt{s}$ being the total energy of the VH system.[148] Associated production of a 0^- boson is a p-wave process with a cross section that scales as β^3, and associated production of a graviton-like 2^+ boson is

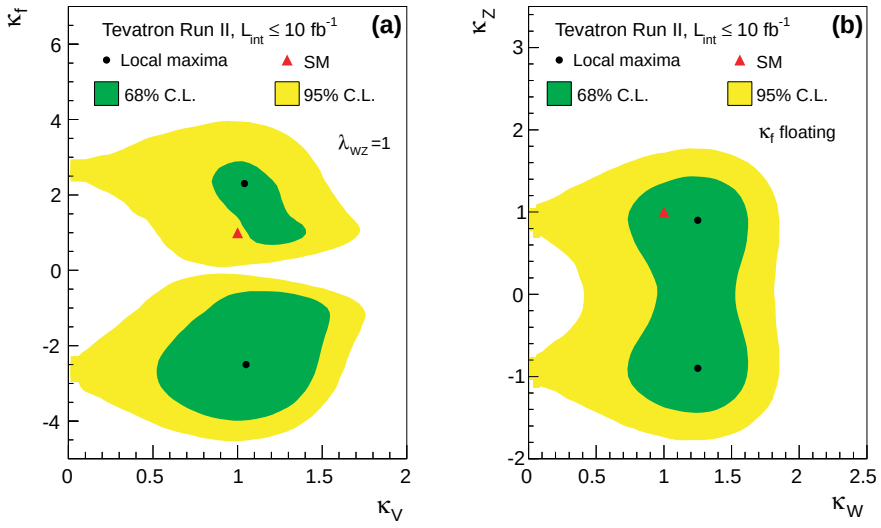

Fig. 10. Two-dimensional constraints in the (κ_V, κ_f) plane (a), and the (κ_W, κ_Z) plane (b), for the combined Tevatron searches for a SM-like Higgs boson with $m_H = 125$ GeV. The points that maximize the local posterior probability densities are marked with dots, and the 68% and 95% C.L. intervals are indicated with the dark- and light-shaded regions, respectively. The SM prediction in each plane is marked with a triangle. From Ref. 13.

a d-wave process with a cross section that scales as β^5. The distribution of the invariant mass of the VX system, where X is either the SM Higgs boson or one of the exotic Higgs-like particles proposed, is therefore quite different, with a much larger average value for the 2^+ particle than for the 0^- particle, with the smallest average value for the SM Higgs boson production. The processes $VX \to Vb\bar{b}$ are used to test for the presence of these exotic bosons, and the observable $m_{Vb\bar{b}}$ is a strong discriminant among the possible signals and also the background processes. Since there is no prediction for the cross section of VX production for the $J^P = 0^-$ and $J^P = 2^+$ particles, nor for the decay branching fractions, the CDF and DØ Collaborations treated this search as a test for an exotic new particle which may either replace the SM Higgs boson or be present along with it.

Strong limits are obtained on the production cross sections times the decay branching ratios $\sigma(VX) \times \mathcal{B}(X \to b\bar{b})$ for the 0^- and 2^+ models. DØ presents the limits in terms of the fraction of the total Higgs boson production rate that could be from the exotic signal, while CDF sets limits on the rate of exotic production. Both collaborations compute p-values for excluding the exotic signals, assuming that the production rates and decay branching fractions are the same for the exotic X bosons as for the SM Higgs boson, obtaining exclusions well in excess of the 95% C.L. assuming this production rate.[14,15]

The CDF and DØ Collaborations have combined the results of these analyses to produce the strongest constraints on these models of exotic bosons.[16] The observed (expected) upper limit on 2^+ boson production is 0.36 (0.33) times the rate predicted for SM Higgs boson production, and the upper limit on 0^- boson production is also 0.36 (0.32) times the SM Higgs boson rate, both assuming that the SM Higgs boson is absent and is replaced with an exotic particle.

Figure 11 shows interpretations allowing for an arbitrary admixture of 0^+ (SM) and exotic Higgs bosons, separately for the combination of searches for the 2^+ boson and the 0^- boson. The signal strength modifiers $\mu_{\rm SM}$, $\mu_{\rm exotic}$ are allowed to vary separatley and the Bayesian posterior probability density is computed for both the 2^+ and 0^- searches. No evidence is seen for either exotic particle, and the data are consistent with the presence of the SM Higgs boson in both cases. Figure 11 also shows the distributions of LLR comparing the hypothesis that the SM Higgs boson is present with its predicted strength and production and decay properties against the hypothesis that the boson is either a $J^P = 2^+$ or 0^- particle, assuming SM Higgs boson production strengths and decay branching ratio to $b\bar{b}$ for the exotic hypotheses. These models are excluded with $\mathrm{CL_s}$ values of 5.6×10^{-7} and 2.6×10^{-7}, respectively.

These searches for exotic $J^P = 2^+$ and 0^- bosons provide independent information about the spin and parity of the Higgs boson from the constraints placed by the ATLAS[149,150] and CMS,[151–155] since they test the $X \to b\bar{b}$ decays instead of $X \to ZZ^{(*)}, WW^{(*)}$, or $\gamma\gamma$ decays.

5. Searches for Higgs Bosons Beyond the Standard Model

The phenomenology of Higgs boson production and decay relevant to searches for Higgs bosons in extensions of the SM is described in Sec. 2.4. While the above extensions of the SM provide useful benchmarks, most searches are designed to be as model-independent as possible.

5.1. *Heavy neutral Higgs bosons decaying to vector bosons*

Searches for a non-SM heavy CP-even neutral Higgs boson decaying to vector bosons have been performed in the context of the SM Higgs boson searches discussed in Secs. 4.5–4.7 (see Ref. 13 for the combined results between CDF and DØ).

Searches for $H \to WW^{(*)}$ and $H \to ZZ^{(*)}$ have been performed in the mass range of m_H =100–300 GeV. The MVA discriminants are retrained at each value of m_H considering only the $gg \to H$ production mode. Searches for $gg \to H \to WW^{(*)}$ and $gg \to H \to ZZ^{(*)}$ are combined assuming the SM prediction for $\mathcal{B}(H \to WW^{(*)})/\mathcal{B}(H \to ZZ^{(*)})$ and 95% C.L. upper limits are derived on $\sigma(H \to WW^{(*)}) \times \mathcal{B}(H \to WW^{(*)})$ as a function of m_H (see Fig. 12(a)). As shown in the same figure, these results can be used to set constraints on models with a sequential fourth generation of fermions (SM4) which, as described in Sec. 2.4, leads to an enhancement in the $gg \to H$ production cross section by a

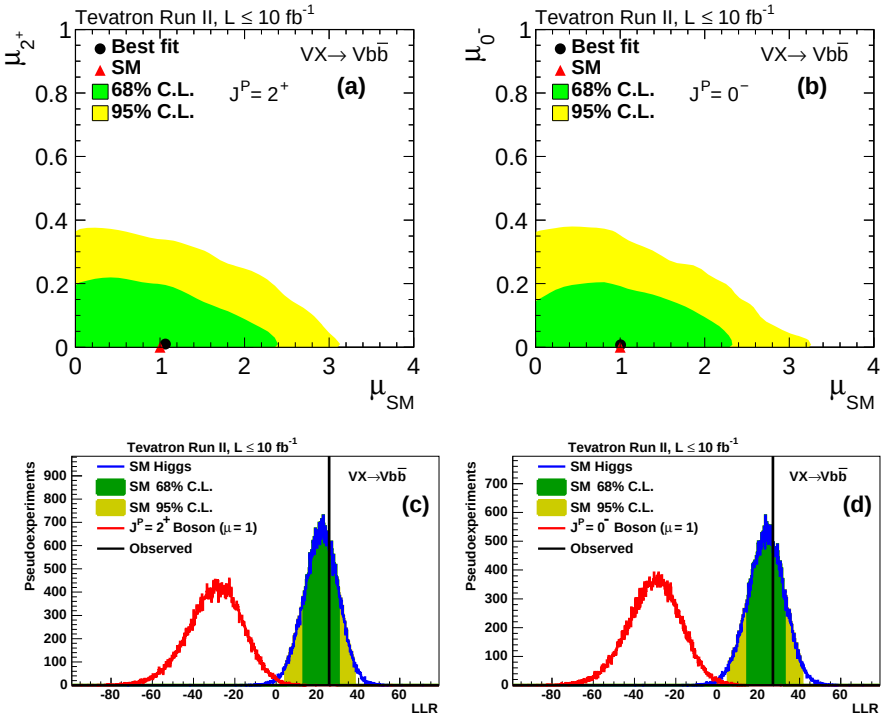

Fig. 11. Two-dimensional constraints in the $(\mu_{\rm SM}, \mu_{\rm exotic})$ plane for exotic models of Higgs boson production with $J^P = 2^+$ (a) and $J^P = 0^-$ (b). Also shown are the expected distributions of LLR comparing the data with the prediction assuming a SM (0^+) Higgs boson against an alternative model with a 2^+ boson produced with SM Higgs boson strength (c), and also for a 0^- boson produced with SM Higgs boson strength (d). From Ref. 16.

factor of ≈ 9. This much larger production cross section provides a model that could be tested with a smaller data sample, and with the complete Run II dataset, a much larger range in m_H could be tested than in the case of the SM. The results are interpreted in the context of two different SM4 scenarios, depending on the assumed masses of the fourth-generation neutrino ($\nu 4$) and charged lepton ($\ell 4$): a "low mass" scenario with $(m_{\nu 4}, m_{\ell 4}) = (80, 100)$ GeV, such that they maximally affect the $H \to WW^{(*)}, ZZ^{(*)}$ branching ratios by opening new decay modes for the Higgs boson, and a "high-mass" scenario with $m_{\nu 4} = m_{\ell 4} = 1$ TeV, where the $H \to WW^{(*)}, ZZ^{(*)}$ branching ratios are unaffected. In the low-mass (high-mass) scenario a Higgs boson with mass in the range 121–225 GeV (121–232 GeV) is excluded at the 95% C.L.

In addition, searches for $H \to \gamma\gamma$ and $H \to WW^{(*)}$ have been performed to probe the existence of a fermiophobic Higgs boson (H_f), as predicted by e.g. Type-I 2HDMs. In the fermiophobic Higgs model (FHM) considered by these searches, the Higgs boson does not couple to fermions at tree level, which leads to substantial modifications to the production cross sections and decay branching ratios. On the

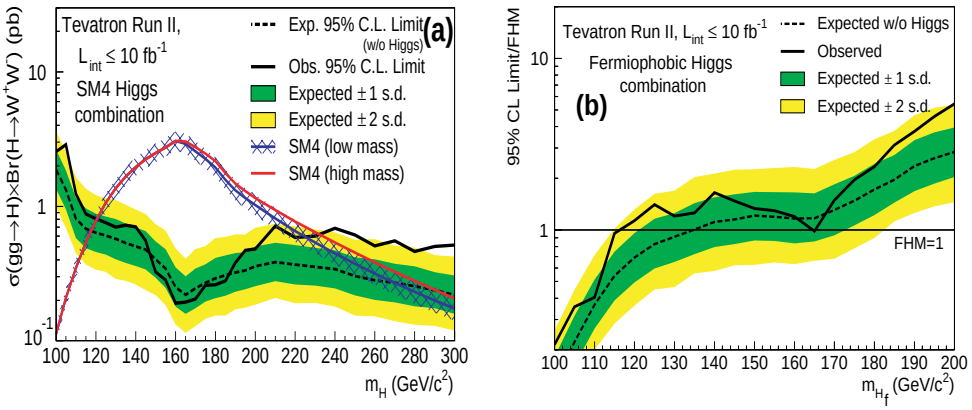

Fig. 12. (a) 95% C.L. upper limits on $\sigma(gg \to H) \times \mathcal{B}(H \to W^+W^-)$ as a function of m_H from the combination of CDF and DØ searches focused on this production and decay mode. Also shown are theoretical predictions for the SM4 in the low- and high-mass scenarios (see text for details). (b) 95% C.L. upper limits on the production cross section of a fermiophobic Higgs boson relative to the FHM prediction as a function of m_{H_f} from the combination of CDF and DØ searches (see text for details). From Ref. 13.

one hand, the process $gg \to H_f$ is suppressed to a negligible level whereas the VH and VBF production modes remain nearly unchanged relative to the corresponding processes in the SM. On the other hand, direct decays to fermions are forbidden, resulting in a large increase to the $H_f \to \gamma\gamma$ branching ratio at low mass relative to the SM decay, while $H_f \to W^+W^-$ dominates over most of the mass range considered. The SM searches for $H \to \gamma\gamma$ and $H \to WW^{(*)}$ have been reoptimized for the FHM scenario by retraining the MVA discriminants after ignoring the gluon-gluon fusion production mechanism, which significantly affects the kinematic distributions of the Higgs boson compared to the SM case. The combined limits from CDF and DØ on Higgs boson production normalized to the FHM predictions are shown in Fig. 12(b) as a function of m_{H_f}. As a result, fermiophobic Higgs bosons in the mass range 100–116 GeV are excluded at the 95% C.L., with an expected excluded mass range of 100-135 GeV.

5.2. *Heavy neutral Higgs bosons decaying to fermions*

As mentioned previously, the MSSM has five physical Higgs bosons: three neutral (h, H and A) and two charged ($H^\pm$). At the leading order, only two parameters are sufficient to describe the Higgs sector, by convention taken to be the ratio of the two Higgs doublets' vacuum expectation values, $\tan\beta$, and the mass of the pseudoscalar boson, m_A. Radiative corrections introduce additional dependencies on other model parameters. At large $\tan\beta$, one of the CP-even Higgs bosons (h or H) is approximately degenerate in mass with the A boson. These two almost-degenerate neutral states are collectively referred to as ϕ. In addition, the couplings

to the down-type fermions are enhanced by a factor of $\tan\beta$ relative to those in the SM. As a result, at high $\tan\beta$ the main decay modes are $\phi \to b\bar{b}$ and $\phi \to \tau^+\tau^-$, with branching ratios of approximately 90% and 10%, respectively. Also, the inclusive ϕ production is dominated by gluon-gluon fusion ($gg \to \phi$, with the b quark playing a potentially important role in the loop) and $b\bar{b} \to \phi$. The latter process may produce a b quark in the detector acceptance, via $gb \to \phi b$, which provides an important experimental handle to suppress backgrounds. The CDF and DØ Collaborations have searched for $\phi \to b\bar{b}$ and $\phi \to \tau^+\tau^-$ in both inclusive and $b\phi$ production modes. A summary of the main features of these searches and their results is provided below.

5.2.1. $\phi \to b\bar{b}$

Searches for $\phi \to b\bar{b}$ have been performed by the CDF and DØ Collaborations, using 2.6 fb^{-1} and 5.2 fb^{-1} of Run II data, respectively.[156,157] An inclusive search for $\phi \to b\bar{b}$ would be extremely difficult due to the overwhelming background from QCD $b\bar{b}$ production. Therefore, these searches are performed in the associated production mode, $b\phi \to bb\bar{b}$, resulting in a signature with at least three b jets in the final state, with the third b jet requirement providing additional rejection against the QCD multijet background. Both CDF and DØ searches employ multijet triggers including b-tagging requirements. After selecting an offline sample with at least three b-tagged jets, the final discriminating variable is the invariant mass of the Higgs boson candidate, defined based on either the two leading b-tagged jets (CDF) or the pairing that maximizes a likelihood-ratio discriminant variable (DØ) (see Fig. 13(a)). In the case of the DØ analysis, the likelihood-ratio discriminant is also used to reject events for which no pairing satisfies a given threshold value, a requirement that helps to further suppress the background. The main challenge of the analysis resides in the modeling of the QCD multijet background, for which no reliable simulation exists. Both analyses build a model of the background in the 3 b-tag sample by using a large data sample requiring exactly two b-tagged jets and applying suitable corrections to account for the change in flavor composition and possible kinematic distortions from the third b-tag requirement.

Different signal hypothesis are tested by varying the Higgs boson mass, m_ϕ, and the individual CDF and DØ analyses find local excesses with significances of 2.8 s.d. at $m_\phi = 180$ GeV and 2.5 s.d. at $m_\phi = 120$ GeV, respectively. These excesses are not significant after taking into account the LEE. Under the assumptions that two out of the three neutral Higgs bosons are degenerate in mass, and that the Higgs boson width is significantly smaller than the experimental resolution, upper limits on the production cross section times branching ratio, $\sigma(gb \to \phi b) \times \mathcal{B}(\phi \to b\bar{b})$ are set as a function of m_ϕ. The cross section is defined such that at least one b quark not originating from the ϕ decay has $p_{\mathrm{T}} > 20$ GeV and $|\eta| < 2.5$. Figure 13(b) shows these upper limits for the combination of the CDF and DØ analyses. In addition, constraints were placed in the ($\tan\beta$, m_A) plane for a particular MSSM benchmark scenario, this time taking into account the Higgs boson width effect. It is

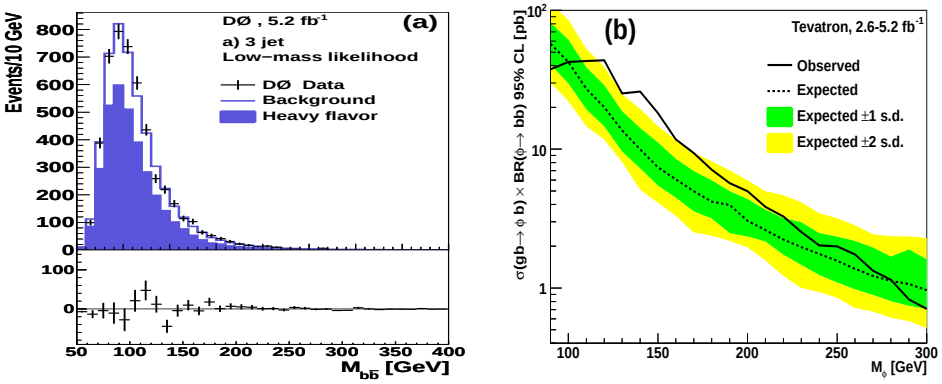

Fig. 13. (a) Distribution of the reconstructed 2-jet invariant mass in the 3 b-tag exclusive channel after the low-mass likelihood requirement in the DØ $b\phi \to bb\bar{b}$ search. The data (points with error bars) are compared to the background prediction, for which the heavy-flavor component (bbb, bbc and bcc) is shown as the shaded region. The lower panel displays the difference between the data and the predicted background. From Ref. 157. (b) Model-independent 95% C.L. upper limits on $\sigma(gb \to \phi b) \times \mathcal{B}(\phi \to b\bar{b})$ from the combination of the CDF and DØ searches as a function of m_ϕ (see text for details). Two out of the three neutral Higgs bosons are assumed to be degenerate in mass and to have a width significantly smaller than the experimental resolution. From Ref. 158.

worth noting that these constraints are strongly dependent on higher-order radiative corrections, a feature not shared by searches for $\phi \to \tau^+\tau^-$, owing to cancellations between radiative corrections affecting the production and decay processes. This makes both searches complementary since their combination could shed light on the nature of a possible signal.

5.2.2. $\phi \to \tau^+\tau^-$

The first search for $\phi \to \tau^+\tau^-$ at a hadron collider was performed by the CDF Collaboration using 86.3 pb^{-1} of data at $\sqrt{s} = 1.8$ TeV collected during Run I.[159] This early search focused on events with one tau decaying to an electron and neutrinos ($\tau \to e\nu_e\nu_\tau$) and the other one decaying hadronically (τ_h), and demonstrated the feasibility to reconstruct the ditau invariant mass when the tau candidates are not back-to-back. Much more sensitive searches were carried out by the CDF and DØ Collaborations during Run II, using up to 1.8 fb^{-1} and 7.3 fb^{-1} of data, respectively.[160–163] Events were selected requiring one or two tau candidates to decay leptonically (excluding ee and $\mu\mu$ final states, which suffer from very large background from Z/γ^* production), resulting in final states denoted as $\tau_e\tau_h$, $\tau_\mu\tau_h$ and $\tau_e\tau_\mu$. The CDF analysis[160] and early DØ analyses[161] considered the three channels, while the final DØ analyses[162,163] were restricted to the $\tau_\mu\tau_h$ channel, which dominates the sensitivity.

While all previous Tevatron searches were focused on the inclusive production

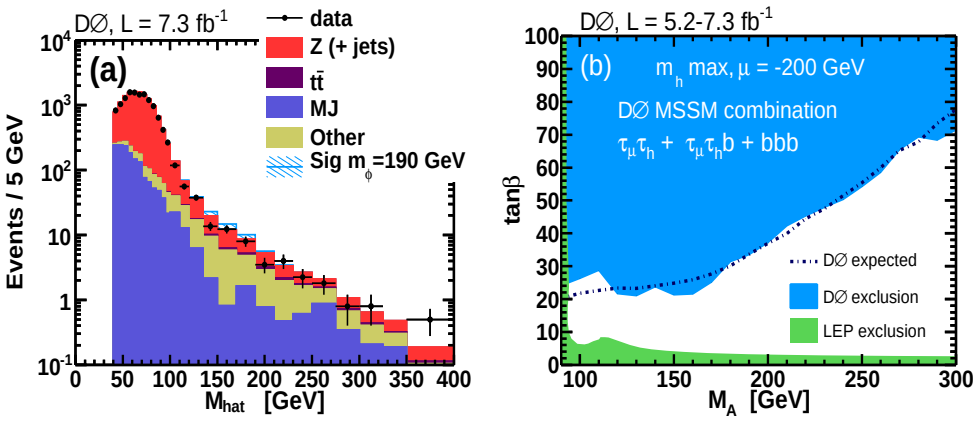

Fig. 14. (a) Distribution of $M_{\rm hat}$ in the inclusive $\tau_\mu\tau_h$ channel from the DØ search (see text for details). The data (points with error bars) are compared to the background prediction, broken down into its individual components. Also shown is the expected contribution from a signal with m_ϕ = 190 GeV. From Ref. 163. (b) Constraints in the ($\tan\beta$,m_A) plane in a given MSSM benchmark scenario from the combination of the final $\phi \to \tau^+\tau^-$ and $\phi \to b\bar{b}$ DØ searches. From Ref. 163.

mode $gg, bb \to \phi$, the final DØ analysis considered both the inclusive and $gb \to \phi b$ associated production modes, by defining two non-overlapping analysis channels without and with the requirement of an additional b-tagged jet, referred to as $\tau_\mu\tau_h$ and $\tau_\mu\tau_h b$, respectively. In the case of the $\tau_\mu\tau_h$ channel, the main background originates from $Z/\gamma^* \to \tau^+\tau^-$, followed by QCD multijet and W+jets production where one of the jets is misidentified as a hadronic tau. The main discriminating variable used is the ditau invariant mass, denoted as $M_{\rm hat}$, defined from the four-momenta of the two leptons and the $\not\!\!E_T$, in such a way that it represents the minimum center-of-mass energy consistent with the decay of a ditau resonance (see Fig. 14(a)). In the case of the $\tau_\mu\tau_h b$ channel, there are large backgrounds from Z/γ^*+jets, $t\bar{t}$ and QCD multijets. Dedicated MVA discriminants are used to reject the $t\bar{t}$ and QCD multijets backgrounds, as well as to discriminate signal from the remaining total background. No significant excess above the SM expectation is found in either of the channels, and constraints in the ($\tan\beta$,m_A) plane in different MSSM benchmark scenarios are derived. Both channels have comparable reach, with the $\tau_\mu\tau_h b$ channel being somewhat more sensitive at lower m_A, owing to the reduced background from $Z/\gamma^* \to \tau^+\tau^-$ by the b-tagging requirement. Figure 14(b) shows the combination of the DØ $\tau_\mu\tau_h$, $\tau_\mu\tau_h b$ channels and the $b\phi \to bb\bar{b}$ search,[157] although the contribution of the latter was very small and strongly dependent on the MSSM parameters assumed.

5.3. *Charged Higgs bosons*

At the Tevatron, charged Higgs bosons can be produced in different modes depending on the value of their mass ($m_{H^\pm}$) compared to the top quark mass. If

$m_{H^+} < m_t - m_b$, the charged Higgs boson can be produced in decays of the top quark, $t \to H^+ b$, competing with the SM decay $t \to W^+ b$. Alternatively, if $m_{H^+} > m_t - m_b$, it can be produced through radiation from a third generation quark or in association with a top quark, such as in the process $q\bar{q}, gg \to t\bar{b}H^-$. Searches at the Tevatron have been performed during Run I and Run II focused on the case of a light charged Higgs boson appearing in top quark decays. At tree level, the branching ratio $\mathcal{B}(t \to H^+ b)$ is simply a function of m_{H^+} and $\tan\beta$. In the MSSM, additional dependencies on the masses and couplings of other supersymmetric particles arise through radiative corrections. The $\mathcal{B}(t \to H^+ b)$ can typically be sizable either at low $\tan\beta$ ($\lesssim 1$) or at high $\tan\beta$ ($\gtrsim 15$). At low $\tan\beta$, H^+ decays predominantly into $c\bar{s}$ for low m_{H^+} ($\lesssim 130$ GeV) and into $t^*\bar{b}$ ($\to W^{+(*)} b\bar{b}$) for higher m_{H^+}. Instead, in the the high $\tan\beta$ regime, H^+ decays into $\tau^+\nu$ almost 100% of the time.

Searches for $t \to H^+ b$ have been performed in $t\bar{t}$ final states either by explicitly seeking an excess of a particular decay mode, such as $t \to H^+ b \to \tau^+\nu b$ or $t \to H^+ b \to c\bar{s}b$, referred to as "appearance" or "direct" searches, or by observing a deficit of a given final state owing to a reduction in its branching ratio as a result of the competing effect from the $t \to H^+ b$ decay, referred to as "disappearance" or "indirect" searches. For instance, for non-zero branching ratio $\mathcal{B}(t \to H^+ b \to c\bar{s}b)$, the number of selected $t\bar{t}$ events is expected to decrease in the ℓ+jets ($\ell = e, \mu$), $\ell\ell'$+jets, $\ell\tau_h$+$\not\!\!E_T$+jets and τ_h+$\not\!\!E_T$+jets final states. Instead, for non-zero branching ratio $\mathcal{B}(t \to H^+ b \to \tau^+\nu b)$, the number of selected $t\bar{t}$ events is expected to increase in $\ell\tau_h$+$\not\!\!E_T$+jets and τ_h+$\not\!\!E_T$+jets final states, while decrease in the rest of final states (see Fig. 15(a)).

Early examples of both types of searches were carried out in Run I. The CDF Collaboration performed an appearance search for $t \to H^+ b \to \tau^+\nu b$ in the $\ell\tau_h$+$\not\!\!E_T$+jets ($\ell = e, \mu$) channel using 106 pb^{-1} of Run I data,[166] setting 95% C.L. upper limits on $\mathcal{B}(t \to H^+ b)$ in the range of 0.5–0.6 for m_{H^+} in the range 60–160 GeV, assuming $\mathcal{B}(H^+ \to \tau^+\nu) = 1$. An appearance search was also performed by the DØ Collaboration using 62 pb^{-1} of Run I data,[167] this time in the more challenging τ_h+$\not\!\!E_T$+jets final state. Finally, the DØ Collaboration also performed a disappearance search by studying the ℓ+jets channel using 109 pb^{-1} of Run I data.[168] In all cases, constraints were set in the ($\tan\beta$, m_{H^+}) plane within the MSSM at tree level.

During Run II, the CDF and DØ Collaborations have performed significantly more sensitive searches by combining multiple analysis channels with and without tau leptons.[164,169] The largest integrated luminosity analyzed in this type of study is by the DØ Collaboration, corresponding to 1 fb^{-1} of data, still only one tenth of the total integrated luminosity recorded in Run II. This search analyzed simultaneously up to 14 channels covering the ℓ+jets ($\ell = e, \mu$), $\ell\ell'$+jets, and $\ell\tau_h$+$\not\!\!E_T$+jets final states. The obtained 95% C.L. upper limits on $\mathcal{B}(t \to H^+ b)$ are in the range $\simeq 0.15$–0.2 depending on the assumed m_{H^+} and scenario considered ($\mathcal{B}(H^+ \to \tau^+\nu) = 1$ or $\mathcal{B}(H^+ \to c\bar{s}) = 1$). Constrains were also set in the ($\tan\beta$, m_{H^+}) plane for different

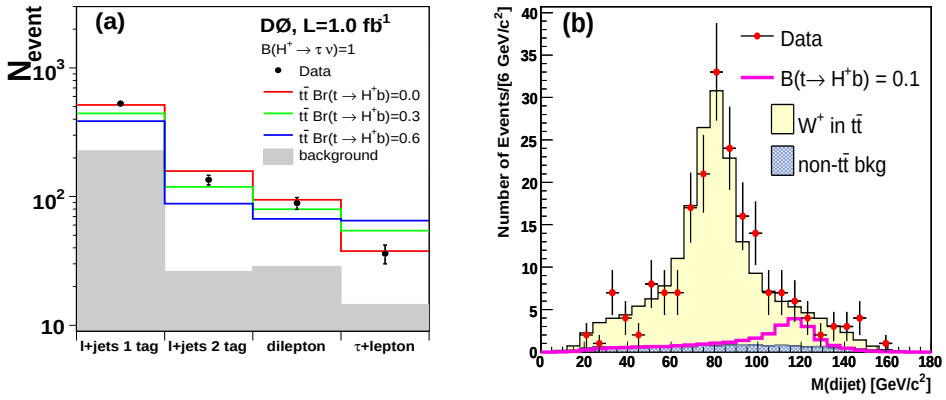

Fig. 15. (a) Distribution of the number of observed events in the different $t\bar{t}$ final states considered by the DØ analysis, compared to the expectation assuming a charged Higgs boson with $m_{H^+} = 80$ GeV decaying exclusively into $\tau^+\nu$ for different values of $\mathcal{B}(t \to H^+b)$. From Ref. 164. (b) Distribution of the dijet mass distribution from the CDF search for $H^+ \to c\bar{s}$ in top quark decays. The data (points with error bars) are compared to the SM prediction and the expected signal contribution from $H^+ \to c\bar{s}$ assuming $m_{H^+} = 120$ GeV and $\mathcal{B}(t \to H^+b)$=0.1. From Ref. 165.

benchmark scenarios.

The most restrictive direct search at the Tevatron for $t \to H^+b \to \tau^+\nu b$ was performed by the CDF Collaboration using 9 fb^{-1} of Run II data.[170] This analysis is focused on the $\ell\tau_h$+$\not\!\!E_T$+jets ($\ell = e, \mu$) channel. A novel feature of this search is the construction of a likelihood discriminant that allows separating the single tau component from the ditau component (where the charged lepton doesn't originate from the W decay but rather from a leptonic tau decay), yielding a direct measurement of $\mathcal{B}(t \to \tau^+\nu b) = 0.096 \pm 0.028$. Under the assumption that $\mathcal{B}(H^+ \to \tau^+\nu) = 1$, this result excludes $\mathcal{B}(t \to H^+b) > 0.059$ at 95% C.L. for m_{H^+} in the range 80–140 GeV.

The CDF Collaboration also performed a direct search for $t \to H^+b \to c\bar{s}b$ using 2.2 fb^{-1} of Run II data.[165] This analysis considers $t\bar{t}$ candidates in the ℓ+jets final state and looks for evidence of the decay $t \to H^+b \to c\bar{s}b$ by performing a kinematic reconstruction of the final state and studying the dijet mass spectrum of the top quark decaying hadronically, where the $H^+ \to c\bar{s}$ would appear as a resonance above the W mass peak (see Fig. 15(b)). No significance excess is found and 95% C.L. upper limits on $\mathcal{B}(t \to H^+b)$ of $\simeq$ 0.1–0.3 are set for m_{H^+} in the range of 60–150 GeV, assuming $\mathcal{B}(H^+ \to c\bar{s}) = 1$.

5.4. *Light CP-odd Higgs bosons*

Although some of the original benchmarks for searches for light CP-odd Higgs bosons (a) arising in singlet extensions of the Higgs sector have changed following the discovery of a SM-like Higgs boson at the LHC, which now could be the lightest

or next-to-lightest CP-even state of the extended Higgs sector, light pseudoscalars are still interesting. On the one hand, a light CP-odd Higgs boson is a potential axion candidate. On the other hand, it can have significant phenomenological implications in the study of an extended Higgs sector: e.g. it can appear in the decay of the SM-like Higgs boson ($h \to aa$), or become a dominant decay mode for a light charged Higgs boson ($H^\pm \to W^{\pm(*)}a$).

The DØ Collaboration has performed searches for the SM Higgs boson decaying to $h \to aa$ using 4.2 fb^{-1} of Run II data.[171] Two different scenarios are considered, depending on the assumed mass of the a boson: (i) for $m_a < 2m_\tau$, both a bosons are searched in decays to $\mu^+\mu^-$, giving a signature with two pairs of collinear muons; (ii) for $2m_\tau < m_a < 2m_b$, one a boson is required to decay to $\mu^+\mu^-$ and the other to $\tau^+\tau^-$, giving a signature of one pair of collinear muons and either large $\not\!\!E_T$ and an additional (not necessarily isolated) muon, or a loosely-isolated electron from $a \to \tau^+\tau^-$ opposite to the muon pair. No significant excess above the background prediction is found in either search and 95% C.L. upper limits on the production cross section times branching ratio are set as a function of m_a, assuming $m_h = 100$ GeV. In the case of the $h \to aa \to 4\mu$ search, the upper limits on $\sigma(h+X) \times \mathcal{B}(h \to aa \to 4\mu)$ are in the range of 10–5.6 fb for m_a in the range of 0.2143–3 GeV. In the case of the $h \to aa \to 2\mu 2\tau$ search, the upper limits on $\sigma(h+X) \times \mathcal{B}(h \to aa \to 2\mu 2\tau)$ are in the range of 19.1–33.7 fb for m_a in the range of 3.6–19 GeV. Assuming no significant difference in selection efficiency between $m_h = 100$ GeV and $m_h = 125$ GeV, these upper limits could be used to set constraints on $\mathcal{B}(h \to aa \to 4\mu)$ and $\mathcal{B}(h \to aa \to 2\mu 2\tau)$ for the SM Higgs boson discovered by the ATLAS and CMS experiments at a mass of ~ 125 GeV.

The CDF Collaboration has searched for an a boson using 2.7 fb^{-1} of Run II data[172] in the context of a search for top quark decays to a charged Higgs boson, $t \to H^+b$, with subsequent decay $H^\pm \to W^{\pm(*)}a$ and $a \to \tau^+\tau^-$. In this case the decay products of the a boson are expected to have low momenta and the new decay mode for the $H^\pm$, if dominant, would make the $H^\pm$ escape existing limits at the Tevatron. The analysis selects $t\bar{t}$ candidates in the ℓ+jets final states, and searches for $a \to \tau^+\tau^-$ decays by looking for at least one isolated track with $3 \le p_{\rm T} \le 20$ GeV in the central detector. The main background to this search is isolated tracks from the underlying event, which are modeled directly from data. By analyzing the $p_{\rm T}$ spectrum of the isolated track and under the assumptions that $\mathcal{B}(H^\pm \to W^{\pm(*)}a) = \mathcal{B}(a \to \tau^+\tau^-) = 1$, 95% C.L. upper limits on $\mathcal{B}(t \to H^+b) < 0.2$ are set for m_{H^+} in the range of 90–160 GeV.

5.5. *Doubly-charged Higgs bosons*

Doubly-charged Higgs bosons ($H^{\pm\pm}$) arise in triplet extensions of the Higgs sector and they couple directly to leptons, photons, W and Z bosons, and singly-charged Higgs bosons. The $H_L^{\pm\pm}$ and $H_R^{\pm\pm}$ bosons respectively couple to left- and right-handed particles, and may have different fermionic couplings. At the Tevatron,

$H^{\pm\pm}$ would be dominantly produced in pairs through the process $q\bar{q} \to Z/\gamma^* \to H^{++}H^{--}$, and decays predominantly to charged leptons if $m_{H^{\pm\pm}} < 2m_{H^{\pm}}$ and $m_{H^{\pm\pm}} - m_{H^{\pm}} < M_W$. Searches at the Tevatron have been performed both for lepton-flavor conserving as well as lepton-flavor violating (LFV) decays, the latter having potentially sizable branching ratios in particular models. These analyses select events consistent with multilepton final states and search for a resonance in the invariant mass of a SS dilepton pair. They typically have very small background rates.

Regarding decays to light-flavor leptons, the CDF Collaboration has searched for $p\bar{p} \to H^{++}H^{--} + X$, with $H^{\pm\pm} \to e^{\pm}e^{\pm}, \mu^{\pm}\mu^{\pm}, e^{\pm}\mu^{\pm}$ using 240 pb^{-1} of Run II data[173] and requiring only a pair of SS leptons of either the same or different flavor. The resulting 95% C.L. lower limits on $m_{H^{\pm\pm}}$ are 133 GeV, 136 GeV and 115 GeV, for exclusive $H_L^{\pm\pm}$ decays to $e^{\pm}e^{\pm}$, $\mu^{\pm}\mu^{\pm}$, and $e^{\pm}\mu^{\pm}$, respectively, and 113 GeV for exclusive $H_R^{\pm\pm}$ decays to $\mu^{\pm}\mu^{\pm}$. The DØ Collaboration has searched for $H^{\pm\pm} \to \mu^{\pm}\mu^{\pm}$ using 1.1 fb^{-1} of Run II data.[174] The resulting 95% C.L. lower limits on $m_{H^{\pm\pm}}$ improve to 150 GeV and 127 GeV for $H_L^{\pm\pm}$ and $H_R^{\pm\pm}$, respectively, both exclusively decaying to $\mu^{\pm}\mu^{\pm}$.

Searches for $H^{\pm\pm}$ decays involving hadronically-decaying tau leptons have also been performed. The CDF Collaboration has searched for LFV decays $H^{\pm\pm} \to \ell^{\pm}\tau^{\pm}$ ($\ell = e, \mu$) using 350 pb^{-1} of Run II data,[175] studying separately events with exactly three or four leptons, where the leading lepton was required to be an electron or muon and there had to be at least one τ_h candidate. The resulting 95% C.L. lower limits on $m_{H^{\pm\pm}}$ are 114 GeV and 112 GeV for exclusive $H_L^{\pm\pm}$ decays to $e^{\pm}\tau^{\pm}$ and $\mu^{\pm}\tau^{\pm}$, respectively. The DØ Collaboration has searched for $H^{\pm\pm} \to \tau^{\pm}\tau^{\pm}, \mu^{\pm}\tau^{\pm}, \mu^{\pm}\mu^{\pm}$ using 7 fb^{-1} of Run II data[176] by selecting events with at least one muon and at least two τ_h candidates. The resulting 95% C.L. lower limits on $m_{H_L^{\pm\pm}}$ are 128 GeV and 144 GeV for exclusive decays to $\tau^{\pm}\tau^{\pm}$ and $\mu^{\pm}\tau^{\pm}$, respectively, and 130 GeV for a model with equal branching ratios into $\tau^{\pm}\tau^{\pm}$, $\mu^{\pm}\tau^{\pm}$ and $\mu^{\pm}\mu^{\pm}$.

Finally, the CDF Collaboration has also considered the scenario in which the lifetime of the $H^{\pm\pm}$ boson is long ($c\tau > 3$ m), resulting in the $H^{\pm\pm}$ boson decaying outside the detector. This search was performed using 292 pb^{-1} of Run II data.[177] The resulting signature is two isolated central tracks leaving large ionization in the tracker and calorimeters and having muon-like penetration properties due to their large mass. The resulting 95% C.L. lower limits on $m_{H^{\pm\pm}}$ are 133 GeV or 109 GeV if only $H_L^{\pm\pm}$ or $H_R^{\pm\pm}$ are kinematically accessible, or 146 GeV if both are degenerate in mass.

5.6. *Higgs boson decays to hidden-sector particles*

The CDF and DØ Collaborations have performed searches for the SM Higgs boson decaying into a pair of "hidden valley" hadrons (HV), each of which in turn decays into a $b\bar{b}$ pair, giving a striking experimental signature of highly displaced

secondary vertices with a very large number of tracks attached from the b-quark decays.[178,179] The CDF and DØ analyses use 3.2 fb^{-1} and 3.6 fb^{-1} of Run II data, respectively. The CDF analysis searches for a pair of jets, where each of them contains a reconstructed secondary vertex, and both jets appear to originate from a common displaced point in space where the HV hadron decayed. The DØ analysis instead requires at least two jets in the event and at least two secondary vertices, and applies stringent requirements on the secondary vertex properties to suppress backgrounds, which are eventually dominated by interactions of particles with the tracker material. In both searches, backgrounds are estimated directly from data. No evidence of a signal is found in either search, and limits on the production cross section of a SM Higgs boson times the branching ratio for $H \to HV\overline{HV} \to b\bar{b}b\bar{b}$ are set, for different values of the Higgs boson mass, the HV mass and its lifetime.

The CDF Collaboration has also performed a generic search for anomalous production of multiple leptons produced in association with W and Z bosons using 5.1 fb^{-1} of Run II data.[180] This search is sensitive to a wide range of scenarios that predict multiple electrons and muons, including clusters of leptons that are produced spatially close to each other, often referred to as "lepton-jets".[181–183] No significant excess is observed above the SM background expectation and a 95% C.L. upper limit on the production cross section is set for a benchmark model in which the Higgs boson decays mainly to a pair of the lightest supersymmetric neutralinos, which in turn decay through a dark sector to lepton-jets.[70,71]

6. Summary and Conclusions

The CDF and DØ Collaborations vigorously sought the Higgs boson predicted by the SM and have produced evidence consistent with such a particle and inconsistent with the background-only prediction with a significance level of 3.1 standard deviations in the $H \to b\bar{b}$ searches in July 2012. As of this writing, the sensitivity of the combined Tevatron analyses remains competitive with results from ATLAS[184] and CMS[185] in the $H \to b\bar{b}$ decay mode, even though the LHC's integrated luminosity is higher per experiment than the Tevatron total, and the center of mass energy is roughly a factor of four higher at the LHC. The fact that the Tevatron was a $p\bar{p}$ collider while the LHC is a pp collider makes the Tevatron results complementary to those of the LHC. Measurements at the Tevatron of the production rates times the decay branching fractions in the $H \to b\bar{b}$, $H \to WW^{(*)}$, $H \to \tau^+\tau^-$, $H \to \gamma\gamma$, and $H \to ZZ^{(*)}$ searches are consistent with the predictions for the SM Higgs boson with a mass of approximately 125 GeV, which is the mass of the Higgs boson observed by ATLAS and CMS. Constraints from CDF and DØ on the couplings and the spin and parity likewise are consistent with the presence of the SM Higgs boson and disfavor exotic interpretations, as well as admixtures of signals from exotic particles and the SM Higgs boson.

Searches for Higgs bosons predicted by extensions of the SM, such as the additional neutral and charged Higgs bosons of the MSSM and other two Higgs doublet

models do not find evidence for any new particles beyond those predicted by the SM.

The searches for Higgs bosons at the Tevatron have been an excellent proving ground for new techniques used to collect, validate, simulate, and analyze hadron collider data, where the expected signal yields are small and the background rates are large and highly uncertain. The use of machine learning techniques and the splitting of data samples into multiple categories with different sensitivities improved the statistical power of the searches. The impact of systematic uncertainties on the results yielded by these new methods was evaluated with techniques common in high-energy physics experiments – validation using control samples and sidebands, as well as propagation of uncertainties in all predictions through the multivariate techniques while handling correlations and uncertainties in the distributions of observable variables. Standard statistical techniques were used to extract final results. These same techniques have been adopted in searches for many new phenomena at the Tevatron and the LHC, as well as measurements of newly established phenomena, such as single top quark production, diboson production, and Higgs boson production.

Acknowledgments

We thank Gregorio Bernardi, Craig Group, and Ken Herner for useful comments and discussions.

We thank the Fermilab staff and technical staffs of the participating institutions for their vital contributions. We acknowledge support from the DOE and NSF (USA), ARC (Australia), CNPq, FAPERJ, FAPESP and FUNDUNESP (Brazil), NSERC (Canada), NSC, CAS and CNSF (China), Colciencias (Colombia), MSMT and GACR (Czech Republic), the Academy of Finland, CEA and CNRS/IN2P3 (France), BMBF and DFG (Germany), DAE and DST (India), SFI (Ireland), INFN (Italy), MEXT (Japan), the KoreanWorld Class University Program and NRF (Korea), CONACyT (Mexico), FOM (Netherlands), MON, NRC KI and RFBR (Russia), the Slovak R&D Agency, the Ministerio de Ciencia e Innovacion, and Programa Consolider–Ingenio 2010 (Spain), The Swedish Research Council (Sweden), SNSF (Switzerland), STFC and the Royal Society (United Kingdom), the A.P. Sloan Foundation (USA), and the EU community Marie Curie Fellowship contract 302103.

References

1. ATLAS Collaboration (G. Aad *et al.*), *Phys.Lett.* **B716**, 1 (2012), `arXiv:1207.7214 [hep-ex]`.
2. CMS Collaboration (S. Chatrchyan *et al.*), *Phys.Lett.* **B716**, 30 (2012), `arXiv:1207.7235 [hep-ex]`.
3. P. W. Higgs, *Phys.Rev.Lett.* **13**, 508 (1964).
4. F. Englert and R. Brout, *Phys.Rev.Lett.* **13**, 321 (1964).
5. G. Guralnik, C. Hagen and T. Kibble, *Phys.Rev.Lett.* **13**, 585 (1964).
6. P. W. Higgs, *Phys.Rev.* **145**, 1156 (1966).

7. S. Glashow, *Nucl.Phys.* **22**, 579 (1961).
8. S. Weinberg, *Phys.Rev.Lett.* **19**, 1264 (1967).
9. A. Salam, *Elementary Particle Theory* , ed: Svartholm, Almqvist & Wiksell, Stockholm (1968).
10. Higgs Working Group Collaboration (M. S. Carena *et al.*) (2000), arXiv:hep-ph/0010338 [hep-ph].
11. CDF and D0 Working Group Members, (L. Babukhadia *et al.*), *Results of the Tevatron Higgs sensitivity study*, FERMILAB-PUB-03-320-E (2003).
12. CDF and D0 Collaborations (T. Aaltonen *et al.*), *Phys.Rev.Lett.* **109**, 071804 (2012), arXiv:1207.6436 [hep-ex].
13. CDF and D0 Collaborations (T. Aaltonen *et al.*), *Phys.Rev.* **D88**, 052014 (2013), arXiv:1303.6346 [hep-ex].
14. D0 Collaboration (V. M. Abazov *et al.*), *Phys.Rev.Lett.* **113**, 161802 (2014), arXiv:1407.6369 [hep-ex].
15. CDF Collaboration (T. Aaltonen *et al.*) (2015), arXiv:1501.04875 [hep-ex].
16. CDF and D0 Collaborations (T. Aaltonen *et al.*) (2015), arXiv:1502.00967 [hep-ex].
17. G. 't Hooft and M. Veltman, *Nucl.Phys.* **B44**, 189 (1972).
18. R. V. Harlander and W. B. Kilgore, *Phys.Rev.Lett.* **88**, 201801 (2002), arXiv:hep-ph/0201206 [hep-ph].
19. C. Anastasiou and K. Melnikov, *Nucl.Phys.* **B646**, 220 (2002), arXiv:hep-ph/0207004 [hep-ph].
20. V. Ravindran, J. Smith and W. L. van Neerven, *Nucl.Phys.* **B665**, 325 (2003), arXiv:hep-ph/0302135 [hep-ph].
21. M. Kramer, E. Laenen and M. Spira, *Nucl.Phys.* **B511**, 523 (1998), arXiv:hep-ph/9611272 [hep-ph].
22. S. Catani, D. de Florian and M. Grazzini, *JHEP* **0105**, 025 (2001), arXiv:hep-ph/0102227 [hep-ph].
23. R. V. Harlander and W. B. Kilgore, *Phys.Rev.* **D64**, 013015 (2001), arXiv:hep-ph/0102241 [hep-ph].
24. S. Catani, D. de Florian, M. Grazzini and P. Nason, *JHEP* **0307**, 028 (2003), arXiv:hep-ph/0306211 [hep-ph].
25. U. Aglietti, R. Bonciani, G. Degrassi and A. Vicini, *Phys.Lett.* **B595**, 432 (2004), arXiv:hep-ph/0404071 [hep-ph].
26. D. de Florian and M. Grazzini, *Phys.Lett.* **B674**, 291 (2009), arXiv:0901.2427 [hep-ph].
27. C. Anastasiou, R. Boughezal and F. Petriello, *JHEP* **0904**, 003 (2009), arXiv:0811.3458 [hep-ph].
28. S. Moch and A. Vogt, *Phys.Lett.* **B631**, 48 (2005), arXiv:hep-ph/0508265 [hep-ph].
29. A. Martin, W. Stirling, R. Thorne and G. Watt, *Eur.Phys.J.* **C63**, 189 (2009), arXiv:0901.0002 [hep-ph].
30. S. Alekhin, S. Alioli, R. D. Ball, V. Bertone, J. Blümlein *et al.* (2011), arXiv:1101.0536 [hep-ph].
31. M. Botje, J. Butterworth, A. Cooper-Sarkar, A. de Roeck, J. Feltesse *et al.* (2011), arXiv:1101.0538 [hep-ph].
32. C. Anastasiou, G. Dissertori, F. Stöckli and B. R. Webber, *JHEP* **0803**, 017 (2008), arXiv:0801.2682 [hep-ph].
33. J. M. Campbell, R. K. Ellis and C. Williams, *Phys.Rev.* **D81**, 074023 (2010),

arXiv:1001.4495 [hep-ph].
34. G. Bozzi, S. Catani, D. de Florian and M. Grazzini, *Phys.Lett.* **B564**, 65 (2003), arXiv:hep-ph/0302104 [hep-ph].
35. G. Bozzi, S. Catani, D. de Florian and M. Grazzini, *Nucl.Phys.* **B737**, 73 (2006), arXiv:hep-ph/0508068 [hep-ph].
36. D. de Florian, G. Ferrera, M. Grazzini and D. Tommasini, *JHEP* **1111**, 064 (2011), arXiv:1109.2109 [hep-ph].
37. I. W. Stewart and F. J. Tackmann, *Phys.Rev.* **D85**, 034011 (2012), arXiv:1107.2117 [hep-ph].
38. J. Baglio and A. Djouadi, *JHEP* **1010**, 064 (2010), arXiv:1003.4266 [hep-ph].
39. G. Ferrera, M. Grazzini and F. Tramontano, *Phys.Rev.Lett.* **107**, 152003 (2011), arXiv:1107.1164 [hep-ph].
40. P. Bolzoni, F. Maltoni, S.-O. Moch and M. Zaro, *Phys.Rev.Lett.* **105**, 011801 (2010), arXiv:1003.4451 [hep-ph].
41. M. Ciccolini, A. Denner and S. Dittmaier, *Phys.Rev.* **D77**, 013002 (2008), arXiv:0710.4749 [hep-ph].
42. W. Beenakker, S. Dittmaier, M. Kramer, B. Plumper, M. Spira *et al.*, *Nucl.Phys.* **B653**, 151 (2003), arXiv:hep-ph/0211352 [hep-ph].
43. W. Beenakker, S. Dittmaier, M. Kramer, B. Plumper, M. Spira *et al.*, *Phys.Rev.Lett.* **87**, 201805 (2001), arXiv:hep-ph/0107081 [hep-ph].
44. L. Reina and S. Dawson, *Phys.Rev.Lett.* **87**, 201804 (2001), arXiv:hep-ph/0107101 [hep-ph].
45. J. Pumplin, D. Stump, J. Huston, H. Lai, P. M. Nadolsky *et al.*, *JHEP* **0207**, 012 (2002), arXiv:hep-ph/0201195 [hep-ph].
46. Particle Data Group Collaboration (J. Beringer *et al.*), *Phys.Rev.* **D86**, 010001 (2012).
47. LHC Higgs Cross Section Working Group, S. Dittmaier, C. Mariotti, G. Passarino and R. Tanaka (Eds.), *CERN-2011-002* (CERN, Geneva, 2011), arXiv:1101.0593 [hep-ph].
48. LHC Higgs Cross Section Working Group, S. Dittmaier, C. Mariotti, G. Passarino and R. Tanaka (Eds.), *CERN-2012-002* (CERN, Geneva, 2012), arXiv:1201.3084 [hep-ph].
49. LHC Higgs Cross Section Working Group, S. Heinemeyer, C. Mariotti, G. Passarino and R. Tanaka (Eds.), *CERN-2013-004* (CERN, Geneva, 2013), arXiv:1307.1347 [hep-ph].
50. A. Djouadi, J. Kalinowski and M. Spira, *Comput. Phys. Commun.* **108**, 56 (Apr 1997).
51. A. Bredenstein, A. Denner, S. Dittmaier and M. M. Weber (2007), arXiv:0708.4123 [hep-ph].
52. The ALEPH, DELPHI, L3 and OPAL Collaborations and the LEP Higgs Working Group, *Phys.Lett.* **B565**, 61 (2003), arXiv:hep-ex/0306033 [hep-ex].
53. OPAL Collaboration (G. Abbiendi *et al.*), *Eur.Phys.J.* **C27**, 311 (2003), arXiv:hep-ex/0206022 [hep-ex].
54. H. P. Nilles, *Phys.Rept.* **110**, 1 (1984).
55. H. E. Haber and G. L. Kane, *Phys.Rept.* **117**, 75 (1985).

56. The ALEPH, DELPHI, L3 and OPAL Collaborations and the LEP Higgs Working Group, *Eur.Phys.J.* **C47**, 547 (2006), arXiv:hep-ex/0602042 [hep-ex].
57. The ALEPH, DELPHI, L3 and OPAL Collaborations and the LEP Higgs Working Group, *Searches for Higgs Bosons Decaying into Photons: Combined Results from the LEP Experiments*, LHWG Note 2002-02 (Jul 2002).
58. The ALEPH, DELPHI, L3 and OPAL Collaborations and the LEP Higgs Working Group (2001), arXiv:hep-ex/0107034 [hep-ex].
59. The ALEPH, DELPHI, L3 and OPAL Collaborations and the LEP Higgs Working Group (2001), arXiv:hep-ex/0107032 [hep-ex].
60. The ALEPH, DELPHI, L3, OPAL, and SLD Collaborations and the LEP Electroweak Working Group, the SLD Electroweak Group, and the SLD Heavy Flavor Group, *Phys.Rept.* **427**, 257 (2006), arXiv:hep-ex/0509008 [hep-ex].
61. CDF and D0 Collaborations (T. Aaltonen *et al.*), *Phys.Rev.* **D86**, 092003 (2012), arXiv:1207.1069 [hep-ex].
62. The CDF and D0 Collaborations and the Tevatron Electroweak Working Group (2012), arXiv:1204.0042 [hep-ex].
63. J. Gunion and H. Haber, *Phys.Rev.* **D67**, 075019 (2003), arXiv:hep-ph/0207010 [hep-ph].
64. G. Branco, P. Ferreira, L. Lavoura, M. Rebelo, M. Sher *et al.*, *Phys.Rept.* **516**, 1 (2012), arXiv:1106.0034 [hep-ph].
65. M. S. Carena, J. R. Ellis, S. Mrenna, A. Pilaftsis and C. Wagner, *Nucl.Phys.* **B659**, 145 (2003), arXiv:hep-ph/0211467 [hep-ph].
66. M. S. Carena, J. R. Ellis, A. Pilaftsis and C. Wagner, *Nucl.Phys.* **B625**, 345 (2002), arXiv:hep-ph/0111245 [hep-ph].
67. S. Chang, R. Dermisek, J. F. Gunion and N. Weiner, *Ann.Rev.Nucl.Part.Sci.* **58**, 75 (2008), arXiv:0801.4554 [hep-ph].
68. M. Strassler and K. M. Zurek, *Phys.Lett.* **B651**, 374 (2007), arXiv:hep-ph/0604261 [hep-ph].
69. M. Strassler and K. M. Zurek, *Phys.Lett.* **B661**, 263 (2008), arXiv:hep-ph/0605193 [hep-ph].
70. A. Falkowski, J. T. Ruderman, T. Volansky and J. Zupan, *JHEP* **1005**, 077 (2010), arXiv:1002.2952 [hep-ph].
71. A. Falkowski, J. T. Ruderman, T. Volansky and J. Zupan, *Phys.Rev.Lett.* **105**, 241801 (2010), arXiv:1007.3496 [hep-ph].
72. B. Holdom, W. Hou, T. Hurth, M. Mangano, S. Sultansoy *et al.*, *PMC Phys.* **A3**, 4 (2009), arXiv:0904.4698 [hep-ph].
73. E. Arik, O. Cakir, S. Cetin and S. Sultansoy, *Acta Phys.Polon.* **B37**, 2839 (2006), arXiv:hep-ph/0502050 [hep-ph].
74. G. D. Kribs, T. Plehn, M. Spannowsky and T. M. Tait, *Phys.Rev.* **D76**, 075016 (2007),

arXiv:0706.3718 [hep-ph].
75. C. Anastasiou, R. Boughezal and E. Furlan, *JHEP* **1006**, 101 (2010), arXiv:1003.4677 [hep-ph].
76. CDF Collaboration (A. Bhatti *et al.*), *Nucl.Instrum.Meth.* **A566**, 375 (2006), arXiv:hep-ex/0510047 [hep-ex].
77. D0 Collaboration (V. M. Abazov *et al.*), *Nucl.Instrum.Meth.* **A763**, 442 (2014), arXiv:1312.6873 [hep-ex].
78. CDF Collaboration (T. A. Aaltonen *et al.*), *Phys.Rev.* **D88**, 092002 (2013), arXiv:1310.0086 [hep-ex].
79. CDF Collaboration (T. Aaltonen *et al.*), *Phys.Rev.* **D89**, 092001 (2014), arXiv:1402.7044 [hep-ex].
80. T. Aaltonen, A. Buzatu, B. Kilminster, Y. Nagai and W. Yao (2011), arXiv:1107.3026 [hep-ex].
81. J. Freeman, T. Junk, M. Kirby, Y. Oksuzian, T. Phillips *et al.*, *Nucl.Instrum.Meth.* **A697**, 64 (2013), arXiv:1205.1812 [hep-ex].
82. CDF Collaboration (D. Acosta *et al.*), *Phys.Rev.* **D72**, 052003 (2005), arXiv:hep-ex/0504053 [hep-ex].
83. CDF Collaboration (A. Abulencia *et al.*), *Phys.Rev.* **D74**, 072006 (2006), arXiv:hep-ex/0607035 [hep-ex].
84. D0 Collaboration (V. Abazov *et al.*), *Nucl.Instrum.Meth.* **A620**, 490 (2010), arXiv:1002.4224 [hep-ex].
85. D0 Collaboration (V. M. Abazov *et al.*), *Phys.Lett.* **B716**, 285 (2012), arXiv:1207.5689 [hep-ex].
86. D0 Collaboration (V. M. Abazov *et al.*), *Nucl.Instrum.Meth.* **A763**, 290 (2014), arXiv:1312.7623 [hep-ex].
87. C. Yuan, *Phys.Rev.* **D41**, 42 (1990).
88. A. Hocker, J. Stelzer, F. Tegenfeldt, H. Voss, K. Voss *et al.*, *PoS* **ACAT**, 040 (2007), arXiv:physics/0703039 [PHYSICS].
89. R. M. Neal, *Bayesian Learning for Neural Networks* (Springer-Verlag New York, Inc., Secaucus, NJ, USA, 1996).
90. M. Feindt and U. Kerzel, *Nucl.Instrum.Meth.* **A559**, 190 (2006).
91. J. Friedman, T. Hastie and R. Tibshirani, *Annals of Statistics* **28**, 2000 (1998).
92. D0 Collaboration (V. Abazov *et al.*), *Phys.Rev.* **D74**, 092005 (2006), arXiv:hep-ex/0609053 [hep-ex].
93. CDF Collaboration (T. Aaltonen *et al.*), *Phys.Rev.* **D82**, 112005 (2010), arXiv:1004.1181 [hep-ex].
94. N. Metropolis, A. W. Rosenbluth, M. N. Rosenbluth, A. H. Teller and E. Teller, *J. Chem. Phys.* **21**, 1087 (Jun 1953).
95. W. Hastings, *Biometrika* **57**, 97 (1970).
96. L. Lyons, *Ann.Appl.Stat.* **2**, 887 (2008).
97. O. J. Dunn, *J.Am.Statist.Assoc.* **56**, 52 (1961).
98. CDF Collaboration (F. Abe *et al.*), *Phys.Rev.Lett.* **81**, 5748 (1998).
99. T. Sjöstrand, S. Mrenna and P. Z. Skands, *JHEP* **0605**, 026 (2006), arXiv:hep-ph/0603175 [hep-ph].
100. CTEQ Collaboration (H. Lai *et al.*), *Eur.Phys.J.* **C12**, 375 (2000), arXiv:hep-ph/9903282 [hep-ph].
101. M. L. Mangano, M. Moretti, F. Piccinini, R. Pittau and A. D. Polosa, *JHEP* **0307**, 001 (2003), arXiv:hep-ph/0206293 [hep-ph].

102. M. L. Mangano, M. Moretti and R. Pittau, *Nucl.Phys.* **B632**, 343 (2002), arXiv:hep-ph/0108069 [hep-ph].
103. F. Maltoni and T. Stelzer, *JHEP* **0302**, 027 (2003), arXiv:hep-ph/0208156 [hep-ph].
104. E. Boos, V. Bunichev, L. Dudko, V. Savrin and A. Sherstnev, *Phys.Atom.Nucl.* **69**, 1317 (2006).
105. R. Brun, F. Carminati, *et al.*, GEANT (1993), CERN Program Library Long Writeup W5013.
106. D0 Collaboration (V. M. Abazov *et al.*), *Phys.Rev.Lett.* **109**, 121804 (2012), arXiv:1208.0653 [hep-ex].
107. CDF Collaboration (T. Aaltonen *et al.*), *Phys.Rev.Lett.* **109**, 111804 (2012), arXiv:1207.1703 [hep-ex].
108. D0 Collaboration (V. M. Abazov *et al.*), *Phys.Rev.* **D88**, 052008 (2013), arXiv:1301.6122 [hep-ex].
109. D0 Collaboration (V. Abazov *et al.*), *Phys.Rev.* **D78**, 012005 (2008), arXiv:0803.0739 [hep-ex].
110. D0 Collaboration (V. Abazov *et al.*), *Phys.Rev.Lett.* **103**, 092001 (2009), arXiv:0903.0850 [hep-ex].
111. CDF Collaboration (T. Aaltonen *et al.*), *Phys.Rev.Lett.* **103**, 092002 (2009), arXiv:0903.0885 [hep-ex].
112. CDF Collaboration (T. A. Aaltonen *et al.*), *Phys.Rev.Lett.* **113**, 261804 (2014), arXiv:1407.4031 [hep-ex].
113. CDF and D0 Collaborations (T. A. Aaltonen *et al.*), *Phys.Rev.Lett.* **112**, 231803 (2014), arXiv:1402.5126 [hep-ex].
114. CDF Collaboration (T. A. Aaltonen *et al.*), *Phys.Rev.Lett.* **112**, 231804 (2014), arXiv:1402.0484 [hep-ex].
115. D0 Collaboration (V. M. Abazov *et al.*), *Phys.Lett.* **B726**, 656 (2013), arXiv:1307.0731 [hep-ex].
116. D0 Collaboration (V. M. Abazov *et al.*), *Phys.Rev.* **D84**, 112001 (2011), arXiv:1108.3091 [hep-ex].
117. D0 Collaboration (V. M. Abazov *et al.*), *Phys.Lett.* **B708**, 21 (2012), arXiv:1110.4592 [hep-ex].
118. D0 Collaboration (V. M. Abazov *et al.*), *Phys.Lett.* **B705**, 313 (2011), arXiv:1105.2788 [hep-ex].
119. CDF Collaboration (T. Aaltonen *et al.*), *Phys.Rev.Lett.* **109**, 111803 (2012), arXiv:1207.1704 [hep-ex].
120. D0 Collaboration (V. M. Abazov *et al.*), *Phys.Rev.Lett.* **109**, 121803 (2012), arXiv:1207.5819 [hep-ex].
121. D0 Collaboration (V. M. Abazov *et al.*), *Phys.Rev.* **D88**, 052010 (2013), arXiv:1303.3276 [hep-ex].
122. CDF Collaboration (T. Aaltonen *et al.*), *Phys.Rev.Lett.* **109**, 111805 (2012), arXiv:1207.1711 [hep-ex].
123. CDF Collaboration (T. Aaltonen *et al.*), *Phys.Rev.* **D87**, 052008 (2013), arXiv:1301.4440 [hep-ex].
124. CDF Collaboration (T. Aaltonen *et al.*), *Phys.Rev.Lett.* **109**, 111802 (2012), arXiv:1207.1707 [hep-ex].
125. D0 Collaboration (V. M. Abazov *et al.*), *Phys.Rev.Lett.* **109**, 121802 (2012), arXiv:1207.6631 [hep-ex].
126. J. M. Campbell and R. K. Ellis, *Phys.Rev.* **D60**, 113006 (1999),

arXiv:hep-ph/9905386 [hep-ph].
127. CDF Collaboration (T. Aaltonen *et al.*), *Phys.Rev.* **D88**, 052013 (2013), arXiv:1301.6668 [hep-ex].
128. D0 Collaboration (V. M. Abazov *et al.*), *Phys.Rev.* **D88**, 052011 (2013), arXiv:1303.0823 [hep-ex].
129. CDF Collaboration (T. Aaltonen *et al.*), *JHEP* **1302**, 004 (2013), arXiv:1208.6445 [hep-ex].
130. CDF Collaboration (T. Aaltonen *et al.*), *Phys.Rev.Lett.* **109**, 181802 (2012), arXiv:1208.2662 [hep-ex].
131. D0 Collaboration (V. M. Abazov *et al.*), *Search for the Standard Model Higgs boson in the* $t\bar{t}H \to t\bar{t}b\bar{b}$ *channel*, D0 Note 5739-CONF (Mar 2009).
132. D0 Collaboration (V. Abazov *et al.*), *Phys.Rev.* **D88**, 052005 (2013), arXiv:1211.6993 [hep-ex].
133. CDF Collaboration (T. Aaltonen *et al.*), *Phys.Rev.Lett.* **108**, 181804 (2012), arXiv:1201.4880 [hep-ex].
134. CDF Collaboration (T. Aaltonen *et al.*), *Phys.Rev.* **D88**, 052012 (2013), arXiv:1306.0023 [hep-ex].
135. D0 Collaboration (V. M. Abazov *et al.*), *Phys.Rev.* **D88**, 052009 (2013), arXiv:1302.5723 [hep-ex].
136. D0 Collaboration (V. M. Abazov *et al.*), *Phys.Rev.* **D88**, 052006 (2013), arXiv:1301.1243 [hep-ex].
137. CDF and D0 Collaborations (T. Aaltonen *et al.*), *Phys.Rev.Lett.* **104**, 061802 (2010), arXiv:1001.4162 [hep-ex].
138. CDF Collaboration (T. Aaltonen *et al.*), *Phys.Rev.Lett.* **104**, 201801 (2010), arXiv:0912.4500 [hep-ex].
139. CDF Collaboration (T. Aaltonen *et al.*), *Phys.Rev.Lett.* **108**, 101801 (2012), arXiv:1112.2978 [hep-ex].
140. D0 Collaboration (V. M. Abazov *et al.*), *Phys.Rev.* **D85**, 112005 (2012), arXiv:1201.5652 [hep-ex].
141. CDF Collaboration (T. Aaltonen *et al.*), *Phys.Rev.* **D86**, 031104 (2012), arXiv:1202.6629 [hep-ex].
142. CDF Collaboration (T. Aaltonen *et al.*), *Phys.Lett.* **B717**, 173 (2012), arXiv:1207.6386 [hep-ex].
143. D0 Collaboration (V. M. Abazov *et al.*), *Phys.Rev.* **D88**, 052007 (2013), arXiv:1301.5358 [hep-ex].
144. CDF Collaboration (T. A. Aaltonen *et al.*), *Phys.Rev.* **D89**, 112001 (2014), arXiv:1403.2300 [hep-ex].
145. CDF Collaboration (T. Aaltonen *et al.*), *Phys.Rev.* **D86**, 072012 (2012), arXiv:1207.5016 [hep-ex].
146. LHC Higgs Cross Section Working Group Collaboration (A. David *et al.*) (2012), arXiv:1209.0040 [hep-ph].
147. J. Ellis, D. S. Hwang, V. Sanz and T. You, *JHEP* **1211**, 134 (2012), arXiv:1208.6002 [hep-ph].
148. D. Miller, S. Choi, B. Eberle, M. Mühlleitner and P. Zerwas, *Phys.Lett.* **B505**, 149 (2001), arXiv:hep-ph/0102023 [hep-ph].
149. ATLAS Collaboration (G. Aad *et al.*), *Phys.Lett.* **B726**, 120 (2013), arXiv:1307.1432 [hep-ex].
150. ATLAS Collaboration (G. Aad *et al.*), *Study of the spin of the new boson with up to 25* fb^{-1} *of ATLAS data* (Apr 2013), ATLAS-CONF-2013-040.

151. CMS Collaboration (S. Chatrchyan *et al.*), *Phys.Rev.* **D89**, 092007 (2014), arXiv:1312.5353 [hep-ex].
152. CMS Collaboration (S. Chatrchyan *et al.*), *JHEP* **1401**, 096 (2014), arXiv:1312.1129 [hep-ex].
153. CMS Collaboration (V. Khachatryan *et al.*), *Eur.Phys.J.* **C74**, 3076 (2014), arXiv:1407.0558 [hep-ex].
154. CMS Collaboration (S. Chatrchyan *et al.*), *Phys.Rev.Lett.* **110**, 081803 (2013), arXiv:1212.6639 [hep-ex].
155. CMS Collaboration (V. Khachatryan *et al.*) (2014), arXiv:1411.3441 [hep-ex].
156. CDF Collaboration (T. Aaltonen *et al.*), *Phys.Rev.* **D85**, 032005 (2012), arXiv:1106.4782 [hep-ex].
157. D0 Collaboration (V. M. Abazov *et al.*), *Phys.Lett.* **B698**, 97 (2011), arXiv:1011.1931 [hep-ex].
158. CDF and D0 Collaborations (T. Aaltonen *et al.*), *Phys.Rev.* **D86**, 091101 (2012), arXiv:1207.2757 [hep-ex].
159. CDF Collaboration (D. Acosta *et al.*), *Phys.Rev.* **D72**, 072004 (2005), arXiv:hep-ex/0506042 [hep-ex].
160. CDF Collaboration (A. Abulencia *et al.*), *Phys.Rev.Lett.* **96**, 011802 (2006), arXiv:hep-ex/0508051 [hep-ex].
161. D0 Collaboration (V. M. Abazov *et al.*), *Phys.Lett.* **B707**, 323 (2012), arXiv:1106.4555 [hep-ex].
162. D0 Collaboration (V. M. Abazov *et al.*), *Phys.Rev.Lett.* **107**, 121801 (2011), arXiv:1106.4885 [hep-ex].
163. D0 Collaboration (V. Abazov *et al.*), *Phys.Lett.* **B710**, 569 (2012), arXiv:1112.5431 [hep-ex].
164. D0 Collaboration (V. Abazov *et al.*), *Phys.Lett.* **B682**, 278 (2009), arXiv:0908.1811 [hep-ex].
165. CDF Collaboration (T. Aaltonen *et al.*), *Phys.Rev.Lett.* **103**, 101803 (2009), arXiv:0907.1269 [hep-ex].
166. CDF Collaboration (T. Affolder *et al.*), *Phys.Rev.* **D62**, 012004 (2000), arXiv:hep-ex/9912013 [hep-ex].
167. D0 Collaboration (V. Abazov *et al.*), *Phys.Rev.Lett.* **88**, 151803 (2002), arXiv:hep-ex/0102039 [hep-ex].
168. D0 Collaboration (B. Abbott *et al.*), *Phys.Rev.Lett.* **82**, 4975 (1999), arXiv:hep-ex/9902028 [hep-ex].
169. CDF Collaboration (A. Abulencia *et al.*), *Phys.Rev.Lett.* **96**, 042003 (2006), arXiv:hep-ex/0510065 [hep-ex].
170. CDF Collaboration (T. A. Aaltonen *et al.*), *Phys.Rev.* **D89**, 091101 (2014), arXiv:1402.6728 [hep-ex].
171. D0 Collaboration (V. Abazov *et al.*), *Phys.Rev.Lett.* **103**, 061801 (2009), arXiv:0905.3381 [hep-ex].
172. CDF Collaboration (T. Aaltonen *et al.*), *Phys.Rev.Lett.* **107**, 031801 (2011), arXiv:1104.5701 [hep-ex].
173. CDF Collaboration (D. Acosta *et al.*), *Phys.Rev.Lett.* **93**, 221802 (2004), arXiv:hep-ex/0406073 [hep-ex].
174. D0 Collaboration (V. Abazov *et al.*), *Phys.Rev.Lett.* **101**, 071803 (2008), arXiv:0803.1534 [hep-ex].
175. CDF Collaboration (T. Aaltonen *et al.*), *Phys.Rev.Lett.* **101**, 121801 (2008), arXiv:0808.2161 [hep-ex].

176. D0 Collaboration (V. M. Abazov *et al.*), *Phys.Rev.Lett.* **108**, 021801 (2012), arXiv:1106.4250 [hep-ex].
177. CDF Collaboration (D. Acosta *et al.*), *Phys.Rev.Lett.* **95**, 071801 (2005), arXiv:hep-ex/0503004 [hep-ex].
178. D0 Collaboration (V. Abazov *et al.*), *Phys.Rev.Lett.* **103**, 071801 (2009), arXiv:0906.1787 [hep-ex].
179. CDF Collaboration (T. Aaltonen *et al.*), *Phys.Rev.* **D85**, 012007 (2012), arXiv:1109.3136 [hep-ex].
180. CDF Collaboration (T. Aaltonen *et al.*), *Phys.Rev.* **D85**, 092001 (2012), arXiv:1202.1260 [hep-ex].
181. J. T. Ruderman and T. Volansky, *JHEP* **1002**, 024 (2010), arXiv:0908.1570 [hep-ph].
182. X. Chen, *JCAP* **0909**, 029 (2009), arXiv:0902.0008 [hep-ph].
183. J. Mardon, Y. Nomura and J. Thaler, *Phys.Rev.* **D80**, 035013 (2009), arXiv:0905.3749 [hep-ph].
184. ATLAS Collaboration (G. Aad *et al.*), *JHEP* **1501**, 069 (2015), arXiv:1409.6212 [hep-ex].
185. CMS Collaboration (S. Chatrchyan *et al.*), *Nature Phys.* **10** (2014), arXiv:1401.6527 [hep-ex].